

# High-energy limit of collision-induced false vacuum decay

---

**Sergei Demidov and Dmitry Levkov**

*Institute for Nuclear Research of the Russian Academy of Sciences,  
60-th October Anniversary Prospect 7a, Moscow 117312, Russia*

*E-mail:* [demidov@ms2.inr.ac.ru](mailto:demidov@ms2.inr.ac.ru), [levkov@ms2.inr.ac.ru](mailto:levkov@ms2.inr.ac.ru)

**ABSTRACT:** We develop a consistent semiclassical description of field-theoretic collision-induced tunneling at arbitrary high energies. As a playground we consider a  $(1+1)$ -dimensional false vacuum decay accompanied by  $N$ -particle collisions at energy  $E$ . The semiclassical suppression exponent  $F_N(E)$  of this process is computed numerically at  $N \gg 1$  and extrapolated to  $N = 2$  with the aid of the Rubakov–Son–Tinyakov conjecture. Our method is based on a specific behavior of  $F_N(E)$ : it decreases with energy, reaches minimum  $F = F_{min}(N)$  at  $E = E_{rt}(N)$  and stays constant at higher energies. The respective cross section is exponentially suppressed at all energies. This behavior is numerically observed in the  $(1+1)$ -dimensional model and conjectured to be general. We show that  $F_{min}(N)$  and  $E_{rt}(N)$  are evaluated using a special class of complex semiclassical solutions which describe exponentially suppressed transitions but nevertheless evolve in real time. Importantly, we argue that the collision-induced transitions with  $N = 2$  initial particles can be described perturbatively at  $E > E_{rt}(2)$  in the background of these solutions, and the terms of the perturbative expansion remain bounded in the high-energy limit. Transitions in the latter regime involve emission of many soft quanta with total energy  $E_{rt}(2)$  by the two colliding particles; the energy excess  $E - E_{rt}(2)$  remains in the initial particles till the end of the process.

**KEYWORDS:** collision-induced tunneling, false vacuum decay, semiclassical methods

---

## Contents

<b>1</b>	<b>Introduction</b>	<b>1</b>
<b>2</b>	<b>Perturbative expansion in the background of a bounce</b>	<b>5</b>
<b>3</b>	<b>From Euclidean to real-time solutions</b>	<b>7</b>
<b>4</b>	<b>Real-time instantons</b>	<b>12</b>
<b>5</b>	<b>Transitions at <math>E &gt; E_{rt}</math></b>	<b>14</b>
<b>6</b>	<b>Stability of perturbative expansion around the real-time instanton</b>	<b>17</b>
<b>7</b>	<b>Perturbative method at high energies</b>	<b>19</b>
<b>8</b>	<b>Summary and discussion</b>	<b>23</b>
<b>A</b>	<b>Multiparticle cross sections</b>	<b>24</b>
<b>B</b>	<b>High-frequency tail of the semiclassical solution</b>	<b>26</b>

---

## 1 Introduction

Exponential suppression of probabilities precludes direct observation of extraordinary tunneling phenomena such as baryon number violation in instanton-like electroweak transitions [1–3] or spontaneous decay of allegedly false Higgs vacuum [4–8]. Quantum mechanical intuition suggests, however, that tunneling probabilities grow with energy. Indeed, tunneling phenomena of the above sort occur at higher rates [9, 10] in two-particle collisions:

$$\sigma(E) \propto e^{-F(E)/g^2}, \quad (1.1)$$

where the suppression exponent<sup>1</sup>  $F(E)$  decreases with collision energy  $E$ , while  $g$  is a small coupling constant. The central question is whether the exponential suppression in Eq. (1.1) disappears at sufficiently high energies and, if it does not, what is the value of the suppression exponent at  $E \rightarrow +\infty$ .

This question is surprisingly nontrivial. Field-theoretic tunneling involves barriers of finite heights  $E_{cb}$  given by the energies of the critical bubble [12–15] and sphaleron [16, 17] in scalar and gauge theories, see Fig. 1a. Nevertheless, the respective collision-induced transitions cannot

---

<sup>1</sup>Dubbed “holy grail function” [11].

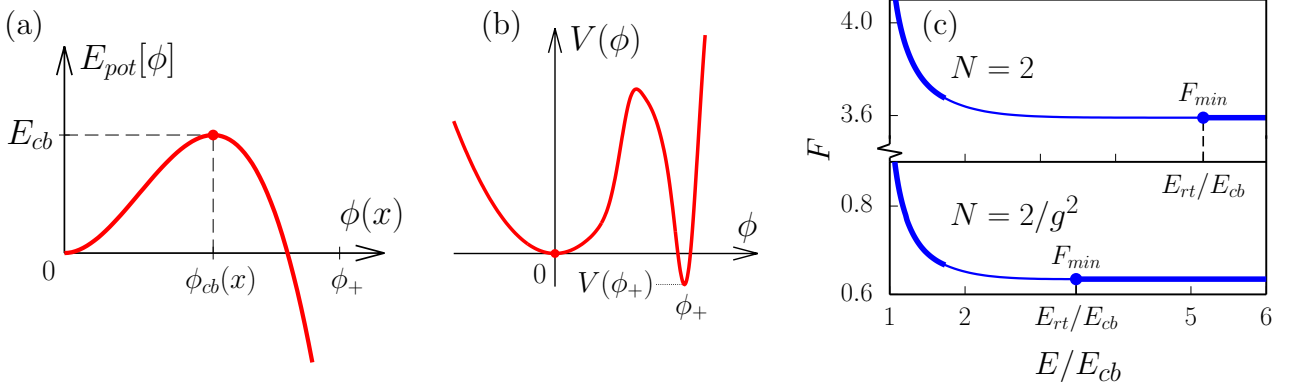


**Figure 1.** (a) A sketch of the potential barrier  $E_{pot}[\phi]$  between the vacua  $\phi = 0$  and  $\phi = \phi_+$ . (b) Scalar potential  $V(\phi)$ . (c) Suppression exponent  $F_N(E)$  at high energies.

become unsuppressed at  $E > E_{cb}$  [18, 19]. Consider e.g. massless fermions  $\psi$  and  $\bar{\psi}$  coupled with small Yukawa constant  $Y$  to the scalar sector of the theory.<sup>2</sup> Their contribution to the scalar self-energy  $\Pi(Q^2)$  obeys dispersion relation [19],

$$\frac{d^2}{(dQ^2)^2} \Pi(Q^2) \Big|_{Q^2 \rightarrow 0} = -\frac{8}{\pi Y^2} \int \frac{dE}{E} \sigma_{tot}(E), \quad (1.2)$$

where<sup>3</sup>  $\sigma_{tot}(E)$  is the total annihilation cross section  $\psi\bar{\psi} \rightarrow \text{anything}$  at the center-of-mass energy  $E$ . If the fermion annihilation leads to unsuppressed over-barrier transitions at  $E > E_{cb}$ , the self-energy  $\Pi(Q^2)$  in Eq. (1.2) receives large nonperturbative contributions at small  $Q^2$ . This would contradict the standard perturbation theory which is valid at low energies. Thus, the cross section (1.1) of collision-induced tunneling is exponentially suppressed at  $E > E_{cb}$ .

In this paper we describe collision-induced tunneling at high energies. To be specific, we consider false vacuum decay in the  $(1+1)$ -dimensional scalar field model

$$S[\phi] = \frac{1}{g^2} \int d^2x \left[ \frac{1}{2} (\partial_\mu \phi)^2 - V(\phi) \right] \quad (1.3)$$

with false and true vacua at  $\phi = 0$  and  $\phi = \phi_+$ , respectively; the scalar potential  $V(\phi)$  is shown in Fig. 1b. We work at weak coupling,  $g \ll 1$ . At zero energy the vacuum  $\phi = 0$  decays spontaneously via formation of expanding bubbles with  $\phi \approx \phi_+$  inside. Below we study the same decay accompanied by a collision of  $N$   $\phi$ -quanta at energy  $E$ . We compute the suppression exponent  $F_N(E)$  of the corresponding inclusive cross section at high energies.

Our numerical result<sup>4</sup> for  $F_N(E)$  is presented in Fig. 1c. This function decreases with energy, reaches minimum  $F_{min}(N)$  at  $E = E_{rt}(N) > E_{cb}$  and stays constant at higher energies. Extrapolating results to the two-particle initial state, we find the same behavior of the exponent  $F(E) \equiv F_2(E)$  in Eq. (1.1) (upper panel in Fig. 1c). We conclude that collision-induced false vacuum decay is exponentially suppressed at arbitrary high energies.

<sup>2</sup>It is straightforward to generalize this argument to other setups.

<sup>3</sup>We ignore irrelevant scalar masses in Eq. (1.2).

<sup>4</sup>In numerical calculations we use a specific potential  $V(\phi)$  which is not significant at the moment.

Energy-independent suppression exponent  $F(E)$  of collision-induced tunneling at high energies was proposed in Ref. [20] and observed in toy models of Refs. [21, 22]. We find the same behavior in the full-fledged field-theoretic model.

Besides, we argue that induced false vacuum decay at threshold  $E = E_{rt}(N)$ , despite being exponentially suppressed, is described by complex semiclassical solutions evolving in real time. The latter solutions were introduced in Ref. [23] under the name *real-time instantons*. The minimal suppression  $F_{min}(N)$  and respective energy  $E_{rt}(N)$  are computed as functionals on these solutions. We argue on general grounds that if the real-time instantons exist for some collision-induced process, the respective suppression exponent is energy-independent and equal to  $F_{min}(N)$  at  $E > E_{rt}(N)$ . Thus, finding the family of these solutions in a given model, one obtains the exponent  $F_N(E)$  in the entire high-energy region  $E > E_{rt}(N)$ .

Most importantly, we show that the real-time instantons serve as backgrounds for the long-awaited [20, 24] perturbative description of collision-induced tunneling at high energies, and the respective corrections are bounded in the high-energy limit. This remarkable feature is in sharp contrast to the properties of perturbative expansions in Euclidean backgrounds [9, 10] which blow up [11, 25][3] at  $E \sim E_{cb}$ . Let us explain the difference by considering scatterings of particles at energy  $\Delta E$  in different backgrounds. At a crude level the quantum particles can be regarded as small-amplitude high-frequency waves  $\delta\phi \propto e^{\pm i\Delta E t}$  added to the background. In the Euclidean case  $\delta\phi$  grows as  $e^{\Delta E \tau}$  and nonlinear backreaction effects become essential at high  $\Delta E$ . In other words, perturbative expansion in  $\delta\phi$  breaks down. In the opposite case of the real-time instanton the waves  $\delta\phi$  evolve adiabatically and do not change the soft background. Scattering of these waves can be described perturbatively.

We support the above observation with explicit calculations. Namely, we propose a working perturbative scheme [26] for evaluating the inclusive cross section of collision-induced tunneling as series in  $g^2$  in the most interesting case of high energies and two initial particles:  $E > E_{rt}(2)$  and  $N = 2$ . One starts with the Green's functions

$$\mathcal{G}_{rt} \equiv \langle \Psi_{rt} | \phi(x_1) \dots \phi(x_{n+2}) | \Psi_0 \rangle = \int \mathcal{D}\phi \Psi_{rt}^*[\phi] \phi(x_1) \dots \phi(x_{n+2}) e^{iS[\phi]} \Psi_0[\phi] \quad (1.4)$$

between the false vacuum  $\Psi_0$  and the most probable final state  $\Psi_{rt}$  of the real-time instanton<sup>5</sup>. One evaluates the path integral in Eq. (1.4) perturbatively in the background of the real-time instanton  $\phi_{rt}^{(N)}$  with  $N$  initial particles: writes

$$\phi(x) \equiv \phi_{rt}^{(N)}(x) + g\delta\phi(x)$$

and expands the integrand in  $g\delta\phi$ . Given the Green's functions, one extracts the amplitudes from the LSZ formula and computes the inclusive cross section. The final result is obtained in the limit  $N \rightarrow 0$  when the initial state of the real-time instanton corresponds to the vacuum initial state in Eq. (1.4).

Our perturbative method is different from the standard instanton expansion in several respects. First, we use real-time instantons as backgrounds. This guarantees stability of the

---

<sup>5</sup>To be specified in the main body of the paper.

perturbative expansion at high energies. Second, we introduce an additional parameter  $N$  of  $\phi_{rt}^{(N)}$  and send  $N \rightarrow 0$  in the end of calculations. Indeed, as  $N \rightarrow 0$  the real-time instanton approaches the formal saddle point of the integral (1.4), but also develops a singularity. We therefore work with smooth configurations  $\phi_{rt}^{(N)}$  and recover<sup>6</sup> correct results for probabilities in the limit  $N \rightarrow 0$ . Third and finally, although below we evaluate only the leading suppression exponent  $F(E) = F_{min}(2)$  at  $E > E_{rt}(2)$ , our perturbative approach can be used for the prefactor and exclusive cross sections at high energies.

With the help<sup>7</sup> of the perturbative method we identify dominant mechanism of the collision-induced transitions at  $E > E_{rt}(2)$  and  $N = 2$ , see Fig. 2. We observe that the colliding particles emit many soft quanta forming a bubble of true vacuum with energy  $E_{rt}(2)$ ; the energy excess  $E - E_{rt}(2)$  remains in the initial particles till the end of the process.

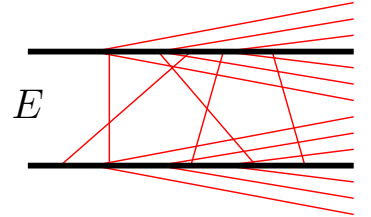


**Figure 2.** Transitions at  $E > E_{rt}(2)$ .

From a general prospective our results support exponential suppression of collision-induced tunneling at arbitrary high energies and per se put on shaky ground proposed searches for non-perturbative phenomena at future colliders [29] or in cosmic ray events [30, 31], cf. Ref. [32]. For example, it was found in Refs. [33, 34] that the suppression exponent of electroweak baryon number violation in two-particle collisions is almost energy-independent at  $E \sim 15$  TeV. If the minimum  $E = E_{rt}(2)$  is somewhere near this point, the respective cross section is suppressed at all energies by a deadly factor  $e^{-F(15 \text{ TeV})/\alpha_W} \sim 10^{-100}$ , where  $\alpha_W$  is the electroweak coupling and we took numerics from Refs. [33, 34]. To get reasonable probabilities, one should consider models with tunneling rates raised by dynamical mechanisms [35–38], resort to strong coupling [39, 40] or exotica [41].

We argued in Ref. [42] that the collision-induced false vacuum decay in  $(1+1)$  dimensions turns into production of kink-antikink pairs from particles once the energy densities of the two vacua are leveled,  $V(0) - V(\phi_+) \rightarrow 0$ . One expects that the properties indicated above hold in this limit. In particular, the cross section of creating a pair of kinks from two particles is exponentially small at all energies, and the suppression exponent of this process does not depend on energy above a certain threshold.

This paper is organized as follows. In Sec. 2 we recall perturbative expansion in the background of a Euclidean bounce. This technique reproduces exponentially growing collision-induced cross section at low energies but breaks down at  $E \gtrsim E_{cb}$ . We proceed with moderate energies in Sec. 3 and demonstrate how the bounce at  $E \ll E_{cb}$  is connected with the real-time instantons at  $E = E_{rt}(N) > E_{cb}$ . The latter semiclassical solutions and transitions at  $E > E_{rt}(N)$  are considered in Secs. 4 and 5, respectively. In Sec. 6 we demonstrate that the same term of perturbative expansion which was exponentially growing with energy in the background of the bounce, gives subdominant and exponentially decreasing with energy contribution in the

<sup>6</sup>This makes our procedure a regularized version of Landau method [27][21, 28] involving singular solutions.

<sup>7</sup>For simplicity we apply the method to the process in a finite volume.

case of the real-time instanton. We propose a working perturbative description of collision-induced tunneling at  $N = 2$  and  $E > E_{rt}(2)$  in Sec. 7. Our results are summarized in Sec. 8.

## 2 Perturbative expansion in the background of a bounce

Let us explain the difficulties with collision-induced tunneling by reviewing its low-energy description [9, 10] in the model (1.3). We will also introduce terminology and sharpen contrast with the high-energy transitions.

Spontaneous decay of false vacuum at  $E = 0$  is described by the celebrated bounce solution [14, 15]  $\phi_b(x)$ , see Fig. 3. The latter has Euclidean and Minkowski parts representing nucleation of a true vacuum bubble and its expansion to infinite size. Note that the bounce is Lorentz-invariant i.e. depends on  $x^2 \equiv x_\mu x^\mu$ . At large negative  $x^2$  it satisfies the Klein-Gordon equation in the false vacuum and therefore behaves as

$$\phi_b(x) \rightarrow \frac{c_b}{2\pi} K_0(m\sqrt{-x^2}) \quad \text{as} \quad x^2 \rightarrow -\infty. \quad (2.1)$$

Here  $m$  is the mass in the false vacuum  $\phi = 0$ . In Eq. (2.1) and below we exploit universal complex time  $t \equiv x^0$  taking real and imaginary values in the respective parts of the contour in Fig. 3. Parameter  $c_b$  is related to the bubble size  $R_b$ :  $\phi_b$  is of order 1 at  $x \sim R_b$ . In the thin-wall limit  $mR_b \gg 1$  one obtains  $c_b \propto e^{mR_b}$ , where the asymptotics of the Bessel function in Eq. (2.1) was used.

To compute the amplitude of collision-induced tunneling, we consider the Green's function

$$\begin{aligned} \mathcal{G}_b &\equiv \langle \Psi_b | \phi(x_1) \dots \phi(x_{n+2}) | \Psi_0 \rangle \\ &= \int \mathcal{D}\phi \, \Psi_b^*[\phi] \, \phi(x_1) \dots \phi(x_{n+2}) \, e^{iS[\phi]} \, \Psi_0[\phi], \end{aligned} \quad (2.2)$$

where  $|\Psi_0\rangle$  and  $|\Psi_b\rangle$  are the false vacuum and the final state of its decay at  $E = 0$ , respectively. The latter describes expanding bubbles.

The idea [9, 10] is to saturate the path integral in Eq. (2.2) with the bounce  $\phi_b(x - x_0)$  treating  $\phi$ 's as prefactors. One obtains,

$$\mathcal{G}_b = \mathcal{A}_b \int d^2x_0 \, \phi_b(x_1 - x_0) \dots \phi_b(x_{n+2} - x_0), \quad (2.3)$$

where we introduced the bounce position  $x_0$ , ignored constant determinant prefactor and denoted the bounce amplitude by  $\mathcal{A}_b = \Psi_b^*[\phi_b] e^{iS[\phi_b]} \Psi_0[\phi_b]$ . The latter amplitude is computed in Refs. [14, 15]: with exponential precision

$$|\mathcal{A}_b|^2 = e^{-2\text{Im} S[\phi_b]}, \quad (2.4)$$

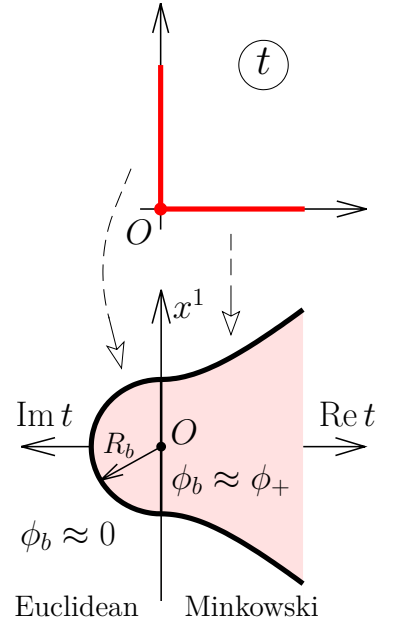


**Figure 3.** Bounce  $\phi_b(x)$ .

in particular,  $|\Psi_b[\phi_b]|, |\Psi_0[\phi_b]| \sim 1$ . Note that the action  $S$  and zero-energy states  $\Psi_0, \Psi_b$  are translation-invariant<sup>8</sup> and therefore independent of  $x_0$ .

Importantly, the large- $x$  asymptotics of the bounce in Eq. (2.1) reproduces correct residual at  $k^2 = m^2$  of its Fourier transform,

$$\phi_b(k) \equiv \int d^2x e^{ik \cdot x} \phi_b(x - x_0) = \frac{ic_b e^{ik \cdot x_0}}{k^2 - m^2 + i\epsilon} + \text{regular part} , \quad (2.5)$$

where we recalled that  $K_0$  in Eq. (2.1) is the Feynman propagator in two dimensions; we denote  $k \cdot x \equiv k_\mu x^\mu$  and assume  $\epsilon \rightarrow +0$ . The residue  $c_b$  in Eq. (2.5) is  $k$ -independent or “point-like” [3]. This property is specific to Euclidean solutions, as we argue below. One immediately obtains the  $2 \rightarrow n$  transition amplitude from the LSZ formula,

$$\mathcal{A}_{2 \rightarrow n} = \mathcal{A}_b \left( \frac{c_b}{g} \right)^{n+2} . \quad (2.6)$$

To derive this expression, we Fourier-transformed Eq. (2.3), extracted the on-shell residues (2.5) and collapsed the integral over  $x_0$  into the  $\delta$ -function<sup>9</sup> representing the energy-momentum conservation. Factors  $g$  in Eq. (2.6) compensate for non-canonical kinetic term in Eq. (1.3).

The amplitude (2.6) exponentially grows with energy  $E$  if the most probable final state contains  $n \approx E/m$  nonrelativistic particles. To confirm this guess about the most probable state, we derive the inclusive cross section in Appendix A,

$$\sigma(E) = \sum_n \int |\mathcal{A}_{2 \rightarrow n}| d\Pi_n = |\mathcal{A}_b|^2 \int d^2\lambda e^{iP \cdot \lambda + \frac{|c_b|^2}{2\pi g^2} K_0(m\sqrt{-\lambda^2 + i\epsilon\lambda^0})} \quad (2.7)$$

where the prefactors are ignored,  $\Pi_n$  is the  $n$ -particle phase space volume and  $P^\mu = (E, 0)$  is the total momentum in the center-of-mass frame. The variable  $\lambda^\mu$  in Eq. (2.7) can be regarded as a typical Compton wavelength of the final particles: the latter become nonrelativistic at  $\lambda \gg m^{-1}$ . At  $g \ll 1$  the integral in Eq. (2.7) is saturated by the saddle point

$$\lambda_s^\mu = (-2iT, 0) , \quad T = \frac{1}{2m} \log \left( \frac{|c_b|^2 \sqrt{m}}{2g^2 E \sqrt{4\pi T}} \right) , \quad (2.8)$$

where the asymptotics of the Bessel function was used. This gives

$$\sigma(E) = e^{(2T+m^{-1})E - 2\text{Im} S[\phi_b]} , \quad (2.9)$$

see Eq. (2.4). In the thin-wall limit  $V(\phi_+) \rightarrow 0$  we substitute  $c_b \propto e^{mR_b}$  and obtain  $T \approx R_b$  with corrections proportional to  $\log(mR_b)$ . The cross section (2.9) in this limit coincides with that in Refs. [43, 44], see also Refs. [45–47].

The result (2.9) demonstrates exponential growth of the cross section with energy. It involves nonrelativistic final particles when  $\lambda_s \sim T$  is large i.e. at  $E \ll m e^{2mR_b}/g^2$ , where

<sup>8</sup>Here and below we assume asymptotic limits  $t_{i,f} \rightarrow \mp\infty$  when all quantities oscillating with the initial  $t_i$  or final  $t_f$  times can be dropped.

<sup>9</sup>It is absorbed in the phase space volume, as usual.



the exponent comes from  $c_b$ . Moreover, the relativistic regime is never reached because at  $E \gtrsim m/g^2$  weak coupling expansion becomes unreliable. Indeed, relative corrections to the leading-order result (2.3) are estimated<sup>10</sup> [3] as  $g^2 n^2$ , where  $n^2$  comes from combinatorics; they are already large at  $n \sim E/m \sim 1/g^2$ . One concludes that correct description of collision-induced tunneling at  $E \gtrsim E_{cb} \sim m/g^2$  should incorporate backreaction of the final-state particles on the semiclassical solution; we will pursue this approach in the next Section.

Let us point at two specific features of the low-energy calculation. First, the bounce residue  $c_b$  in Eq. (2.5) does not depend on  $k$  as  $k \rightarrow +\infty$ . Second, the final state  $\Psi_b$  has zero energy and factorizes in Eq. (2.3). We will see that these two properties do not hold for perturbative expansion about the relevant high-energy solutions.

### 3 From Euclidean to real-time solutions

We demonstrated that collision-induced transitions are no longer described by the bounce at  $E \gtrsim E_{cb}$ . Since our interest is in high energies, we set this background aside and search for true semiclassical solutions saturating the inclusive probabilities of false vacuum decay induced by  $N$ -particle collisions

$$\sigma_N(E) = \sum_{\Psi_i, \Psi_f} \left| \langle \Psi_f | \hat{U}(t_f, t_i) | \Psi_i; E, N \rangle \right|^2 \sim e^{-F_N(E)/g^2}, \quad (3.1)$$

where  $\hat{U}$  is the evolution operator,  $t_{i,f} \rightarrow \mp\infty$ , and in the second equality we introduced the suppression exponent  $F_N(E)$ . The sum in Eq. (3.1) runs over all initial states  $\Psi_i$  with energy  $E$  and multiplicity  $N$  in the false vacuum and final states  $\Psi_f$  containing a bubble of true vacuum. Importantly,  $\sigma_N(E)$  coincides at  $N = 2$  with the two-particle collision-induced cross section  $\sigma(E)$  and can be computed semiclassically at  $N \gg 1$ . Moreover, Rubakov–Son–Tinyakov conjecture [50] states that the suppression exponent  $F_N(E)$  does not depend on  $N$  at  $N \ll 1/g^2$ , see Refs. [51–54] for confirmations. This means that the two-particle exponent  $F(E)$  in Eq. (1.1) is obtained by extrapolating the semiclassical result for  $F_N(E)$  to  $g^2 N \rightarrow 0$ .

In direct semiclassical approach one writes a path integral for  $\sigma_N(E)$  and saturates it at  $g \ll 1$  by the saddle-point configuration  $\phi_s(x)$ . In general, this configuration is complex. The saddle-point equations for  $\phi_s$  are summarized in Fig. 4a, see Ref. [50] for derivation. Like the bounce, this configuration satisfies the classical field equations along the complex time contour, and contains an expanding bubble in the asymptotic future  $t \rightarrow +\infty$  where the solution is real. Peculiarities of  $\phi_s(x)$  are related to the nontrivial initial state in Eq. (3.1). Along the part  $AB$  of the contour the semiclassical solution describes motion of free particles prior to the collision: in the asymptotic past it reduces to free waves

$$\phi_s(x) \rightarrow \int \frac{dk}{4\pi\omega_k} (a_k e^{-ik \cdot x} + b_k^* e^{ik \cdot x}) \quad \text{as} \quad t \rightarrow -\infty, \quad (3.2)$$

---

<sup>10</sup>Sophisticated resummation [48, 49] shows that the true expansion parameter is  $g^2 n \ll 1$ .



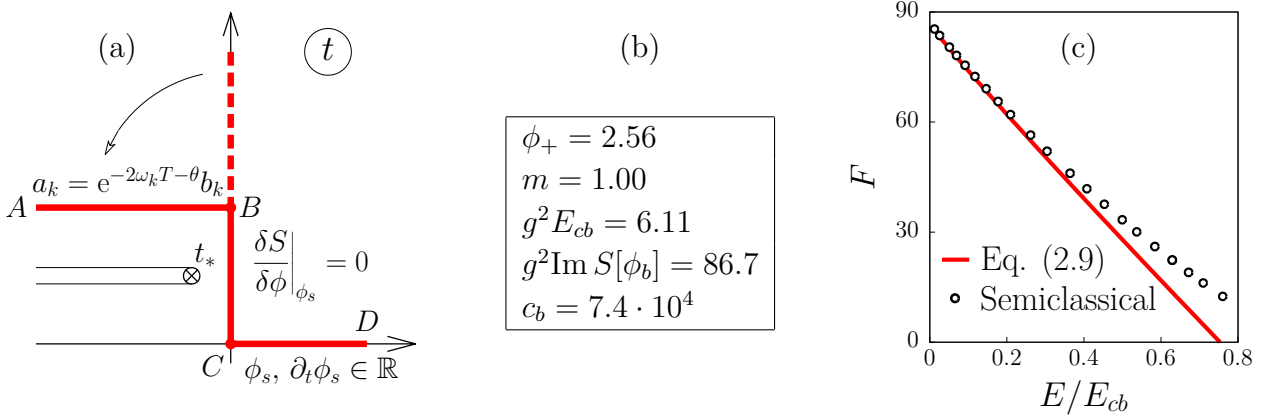


**Figure 4.** (a) Boundary value problem for  $\phi_s(x)$ . (b) Physical quantities in the model (3.7). (c) Suppression exponent at low energies.

where  $k^\mu = (\omega_k, k)$ ,  $\omega_k^2 = k^2 + m^2$ , and the limit is taken along the time contour of Fig. 4a. In Eq. (3.2) we introduced the classical counterparts  $a_k, b_k^*$  of the annihilation and creation operators with relativistic normalization. They are related by the initial condition

$$a_k = e^{-2\omega_k T - \theta} b_k^* \quad (3.3)$$

involving two Lagrange multipliers  $T$  and  $\theta$  due to fixation of energy  $E$  and the number  $N$  of colliding particles. The latter quantities are given by the standard expressions

$$g^2 E = \int dk \frac{a_k b_k^*}{4\pi}, \quad g^2 N = \int dk \frac{a_k b_k^*}{4\pi\omega_k}. \quad (3.4)$$

In the limit  $T \rightarrow +\infty$  Eq. (3.3) reduces to vacuum condition  $a_k = 0$  which corresponds to  $E = N = 0$ . In this case  $\phi_s(x)$  coincides with the bounce solution  $\phi_b(x)$ . At finite  $T$  and  $\theta$  the saddle-point solution describes transition at nonzero  $E$  and  $N$ . In what follows we solve equations in Fig. 4a and relate  $(T, \theta)$  to  $(E, N)$  by Eq. (3.4).

Given the saddle-point configuration  $\phi_s(x)$ , one evaluates the suppression exponent [50]

$$F_N(E) = g^2(2\text{Im } S[\phi_s] - 2ET - N\theta) + \text{Im} \int dx \phi_s \partial_t \phi_s \Big|_{t=t_i}, \quad (3.5)$$

where the last three terms are the initial-state contributions. Importantly, the method of Lagrange multipliers implies the Legendre transform

$$\partial_E F_N(E) = -2g^2 T, \quad \partial_N F_N(E) = -g^2 \theta, \quad (3.6)$$

which demonstrates that  $T$  and  $\theta$  are proportional to the derivatives of  $F_N(E)$ .

We solve the boundary value problem in Fig. 4a numerically. To this end we specify the scalar potential in dimensionless units,

$$V(\phi) = \frac{\phi^2}{2} \left[ 1 - vW \left( \frac{\phi - 2}{u} \right) \right], \quad (3.7)$$

where  $W(x) = e^{-x^2}(x + x^3 + x^5)$ ,  $u = 0.4$ , and the energy density  $V(\phi_+) = -0.4$  of the true vacuum is set by tuning  $v \approx 0.84$ . Function (3.7) is plotted in Fig. 1b. It is almost quadratic at  $\phi < \phi_+/2$  and nontrivial at larger  $\phi$ , so that waves in Eq. (3.2) remain linear<sup>11</sup> almost up to their collision point.

We computed physical quantities in the model (3.7), see Fig. 4b. To this end we have numerically found the bounce  $\phi_b(t, x)$  and the critical bubble  $\phi_{cb}(x)$ , see Ref. [15] for details. Recall that the bounce action  $2\text{Im } S[\phi_b]$  in Eq. (2.4) is the suppression exponent of false vacuum decay at zero energy, whereas the energy  $E_{cb}$  of the critical bubble gives the height of the potential barrier between the vacua. We also extracted the bounce residue  $c_b$  from the asymptotics of  $\phi_b(t, x)$  at  $x_\mu x^\mu \rightarrow -\infty$ , see Eq. (2.1). We remind that the coupling constant  $g \ll 1$  scales out in the semiclassical calculations, cf. Eq. (1.3).

We solve the semiclassical boundary value problem for  $\phi_s(t, x)$  numerically. To this end we discretize equations in Fig. 4a and introduce uniform  $N_t \times 2N_x$  lattice with sites  $t_i$  and  $x_j$  covering the contour  $ABCD$  and space interval<sup>12</sup>  $(-L, L)$ ,  $L = 7$ ; the spatial lattice spacing is  $\Delta x \equiv L/N_x$ . We use the second-order finite-difference approximation for the field equation and trade Fourier transform in Eq. (3.2) for its discrete version. This turns the semiclassical boundary value problem into a set of  $N_t \times 2N_x$  nonlinear algebraic equations<sup>13</sup> for  $\phi_{ij} = \phi_s(t_i, x_j)$  which are solved by the Newton-Raphson method [55]. Detailed description of our numerical technique will be presented elsewhere [56], see Refs. [57][33] for related works. In the subsequent Sections we will concentrate on numerical solutions at high energies and small multiplicities. We will need large  $N_t$  and  $N_x$  because the typical frequencies  $\omega_k \sim E/N$  of these solutions are high. In particular, lattices  $N_t \times N_x = 3000 \times 150$  and  $11000 \times 4000$  are required to reach acceptable numerical precision at  $E \sim E_{cb}$  and the highest energies, respectively.

The starting point of our numerical procedure is the bounce  $\phi_b(t, x)$  which satisfies the boundary value problem in Fig. 4a at  $T = +\infty$  and  $E = N = 0$ . We decrease  $T$  at  $\theta = 0$  in small steps finding one solution  $\phi_s(t, x)$  at a time. We compute the energy  $E$  and initial particle number  $N$  of each solution by Eqs. (3.4). These solutions are marked by red (dark) points in the  $(E, N)$  plane in Fig. 5 (central panel). At energies somewhat below  $E_{cb}$  we switch to  $\theta = 0.4$  (green (light) points) and continue decreasing  $T$  until the solution with  $T = 0$  is reached (squared point). The latter solution  $\phi_s = \phi_{rt}(t, x)$  is called “real-time instanton.”

At low energies our semiclassical solutions reproduce the results of the previous Section. Indeed, Fig. 4c compares the semiclassical exponent (3.5) at  $\theta = 0$  (points) with the exponent in Eq. (2.9) (line), where the values in Fig. 4b are used. The two graphs coincide at  $E \ll E_{cb}$  despite the fact that the perturbative results are obtained at  $N = 2$  whereas the semiclassical solutions involve large multiplicities  $N \sim 1/g^2$ , see Fig. 5. This is because  $F_N(E)$  is independent<sup>14</sup> of  $N$  at  $E < E_{cb}$  [44], so we do not have to continue it to  $g^2 N \rightarrow 0$ . Importantly, the perturbative graph in Fig. 4c becomes negative at  $E \approx 0.8E_{cb}$  indicating apparent violation

<sup>11</sup>Long nonlinear evolution in other models is costly for numerical computations.

<sup>12</sup>Larger intervals are used at low energies due to larger sizes of the respective solutions.

<sup>13</sup>The solutions are  $P$ -symmetric,  $\phi_s(t, x) = \phi_s(t, -x)$ , so we use only a half of the lattice with  $x_j > 0$ .

<sup>14</sup>In the thin-wall approximation which works well [42] at  $V(\phi_+) = -0.4$ .

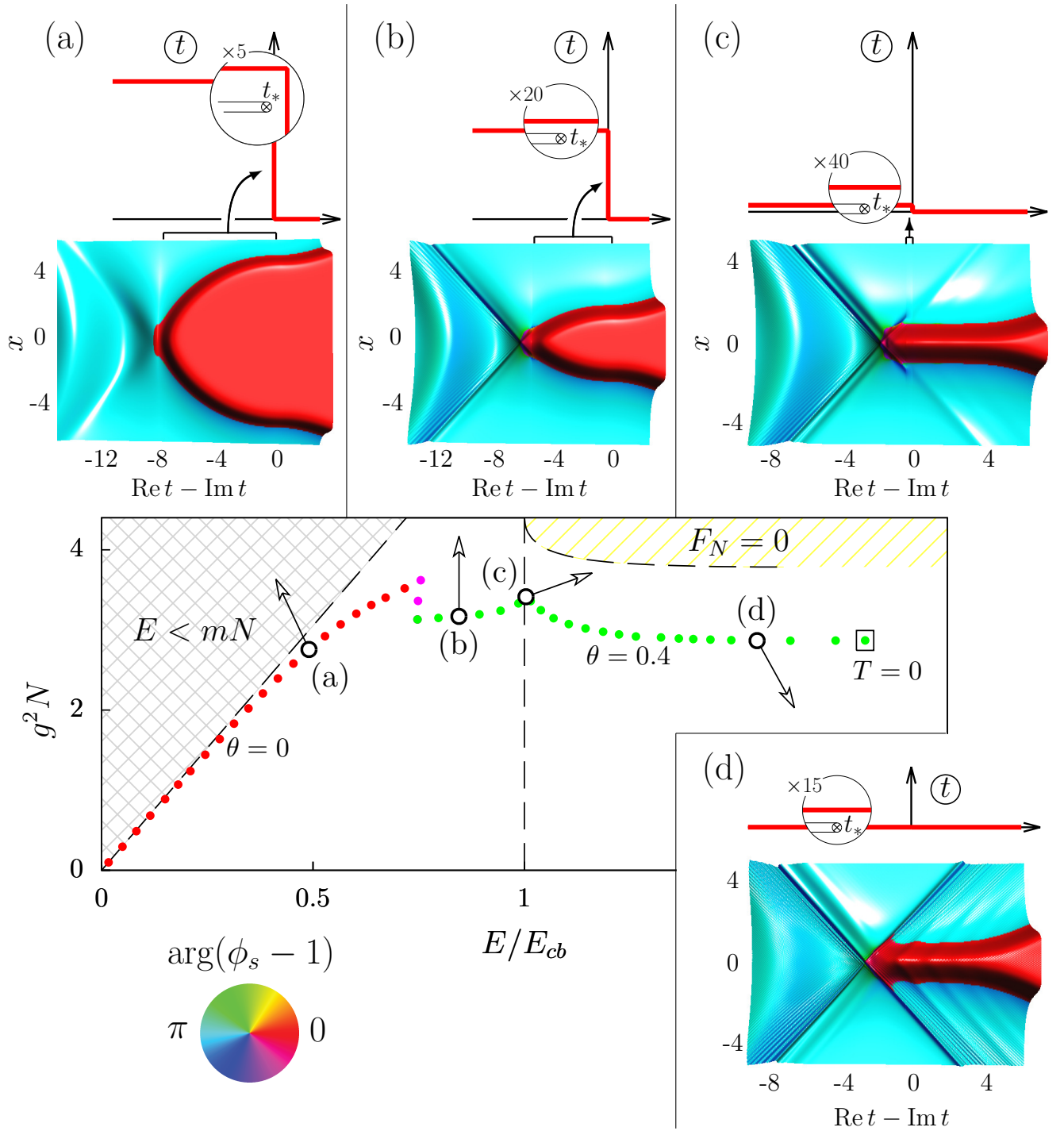


**Figure 5.** Central plot:  $(E, N)$  plane of initial data. Insets (a)—(d): Solutions  $\phi_s(t, x)$  and their  $t$ -contours. Color marks  $\arg(\phi_s - 1)$ , singularities  $t = t_*$  of the solutions are indicated in the zoomed areas. The lattice size is  $N_t \times N_x = 3000 \times 150$ .

of unitarity. At these energies the perturbative expansion of Sec. 2 is not reliable unlike the semiclassical method of this Section.

One observes a dramatic change in the form of the saddle-point solutions at  $E \approx E_{cb}$ .

The low-energy solutions in Figs. 5a,b resemble the bounce: they contain long Euclidean parts and describe creation of true vacuum bubbles (the latter are shown by red (dark) in figures). Waves in the left parts of the plots represent initial particles. In contrast, at  $E > E_{cb}$  the initial waves are sharp and the bubbles are small, see Figs. 5c,d. Another property of high-energy solutions is small durations of their Euclidean evolutions and, nevertheless, nonzero values of the suppression exponents<sup>15</sup> (3.5) thanks to complex-valued  $\phi_s(t, x)$ . In particular, the real-time instanton at  $T = 0$  evolves entirely along  $t \in \mathbb{R}$ . We will argue that this feature guarantees stable perturbative expansion at high energies.

One wonders how the durations of Euclidean evolutions can be of any physical meaning: they are not even explicitly specified in Fig. 4a. Indeed, one expects that  $\phi_s(t, x)$  are analytic functions of time which can be continued to any contours. But in fact, the solutions and, in particular, the bounce have branch-cut singularities starting at  $t = t_*$  which separate their time contours from the real time axis, see Fig. 4a. We compute positions of these singularities for the solutions (a)–(d) in Fig. 5. To this end we continue  $\phi_s(t, x)$  to complex  $t$  and find the points  $t = t_*$  where  $|V(\phi_s)| = \infty$ , see the zoomed areas in the respective  $t$ -planes. The singularities prevent us from continuing the low-energy solutions to the real time axis. We find, however, that  $\text{Im } t_*$  decreases with energy and becomes negative for the solution (d) in Fig. 5. The latter solution can be considered in real time, as well as the real-time instanton at  $T = 0$ .

We find the semiclassical solutions at  $g^2 N = 2$  (not shown in Fig. 5) and plot the respective suppression exponent  $F_N(E)$  in Fig. 1c (thick line in the left part of the lower panel). The latter exponent monotonously decreases with energy until the point  $T = 0$  and  $E = E_{rt}(N)$  is reached<sup>16</sup>. The region of few-particle initial states  $N \ll 1/g^2$  cannot be directly addressed at the present-day computers. So, we extrapolate numerical results into this region. Since  $e^{-\theta}$  analytically enters the semiclassical equations in Fig. 4a, the particle number  $N$ , action  $S[\phi_s]$ , and the last term in Eq. (3.5) have regular Taylor expansions in this parameter. Moreover,  $e^{-\theta} \rightarrow 0$  leads to Feynman boundary conditions at  $t \rightarrow -\infty$  and therefore to  $g^2 N \rightarrow 0$ , see Eq. (3.3). Substituting all Taylor expansions into Eq. (3.5) and using Eq. (3.6), one finds that  $F_N(E) + g^2 \theta N + g^2 N = F(E) + O(g^4 N^2)$ . We fit numerical data for the left-hand side of this equality with function  $F(E) + d(E) \cdot g^4 N^2$  and obtain the suppression exponent  $F(E)$  (solid line in the left upper part of Fig. 1c). Numerical error of this procedure is expected to be smaller than 5%. Our results show that the two-particle exponent  $F(E)$  is also a decreasing function of energy.

We finish this Section by remarking that the above semiclassical solutions describe classically forbidden transitions from the initial states with relatively small multiplicities  $N$ . Increasing  $N$ , one reaches the states decaying classically (region “ $F_N = 0$ ” in Fig. 5). Classical transitions in the model (3.7) were studied in Ref. [60], see Refs. [35–37] for the related work.

<sup>15</sup>Exponentially suppressed transitions at  $E > E_{cb}$  are called “dynamical tunneling” [58, 59] to distinguish from potential tunneling at low energies.

<sup>16</sup>Data lines are not shown at high energies where the numerical errors are large. To decrease the computational cost, we find the solution at  $E = E_{rt}$  at high precision (next Section) and fill the gap with thin interpolating line.

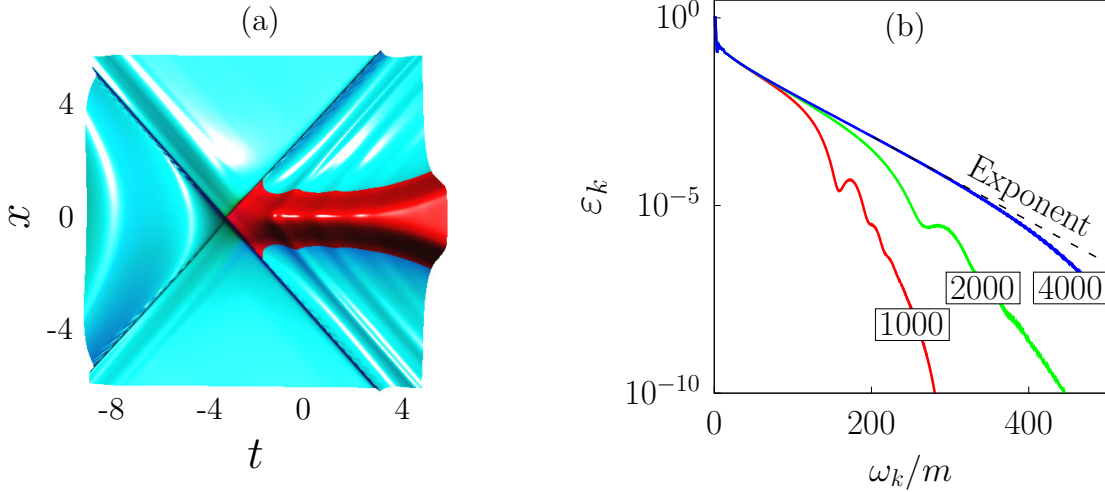


**Figure 6.** (a) Real-time instanton  $\phi_{rt}(t, x)$  and (b) its initial energy distributions  $\varepsilon_k$  at different  $N_x$  (numbers in boxes). In both figures  $\theta = 0.199$ ,  $(E, N) \approx (2.4 E_{cb}, 3.5/g^2)$ ,  $N_t = 11000$ . Figure (a) uses colors of Fig. 5 and  $N_x = 2000$ .

## 4 Real-time instantons

Solutions of the saddle-point equations at  $T = 0$  and arbitrary  $\theta$  are special in many respects, see one of them in Fig. 6a. At a given  $N$  they have the highest energies  $E = E_{rt}(N)$  and smallest suppression exponents  $F_{min}(N) \equiv F_N(E_{rt}(N))$  considered so far. Indeed, in the previous Section we raised the energy of solutions by decreasing  $T$  from  $T = +\infty$  to  $T = 0$ . The exponent  $F_N(E)$  was decreasing because  $\partial_E F_N = -2g^2 T < 0$ , see Eq. (3.6). At  $E = E_{rt}$  it reached extremum  $\partial_E F_N = 0$ . In Sec. 5 we will argue that this extremum is a global minimum: specifically,  $F_N(E)$  is energy-independent at  $E > E_{rt}(N)$ .

Another important feature came as a surprising numerical fact in Fig. 5: the real-time instantons  $\phi_{rt}(t, x)$  are defined along the real time axis  $t \in \mathbb{R}$ . Technically, this property is related to the initial condition (3.3). Indeed, the positive- and negative-frequency terms in the integrand of Eq. (3.2) are of order  $\tilde{b}_k^* \equiv b_k^* e^{-\omega_k T_{AB}}$  and  $\tilde{a}_k \equiv a_k e^{\omega_k T_{AB}}$ , where  $T_{AB} = \text{Im } t_{AB}$  is the height of the time contour. The integrals of these terms in Eq. (3.2) converge faster at larger and smaller  $T_{AB}$ , respectively. At  $T_{AB} = T$  the terms are of the same order because  $\tilde{a}_k = e^{-\theta} \tilde{b}_k$  due to the initial condition (3.3). This “optimal” contour lies right in the middle between the singularities of the solution: at somewhat higher or lower  $T_{AB}$  one of the integrals in Eq. (3.2) diverges signaling that the contour hits the singularity. We use  $T_{AB} = T$  in numerical calculations and show the corresponding contour in Figs. 5a–d. At  $T \rightarrow 0$  our optimal contour coincides with the real time axis.

The above argument turns quantitative if we use the high-frequency asymptotics of the solution. Namely, consider the energy of modes with wave number  $k$  in Eq. (3.4),

$$\varepsilon_k \equiv \frac{a_k b_k^*}{4\pi}, \quad g^2 E = \int dk \varepsilon_k. \quad (4.1)$$

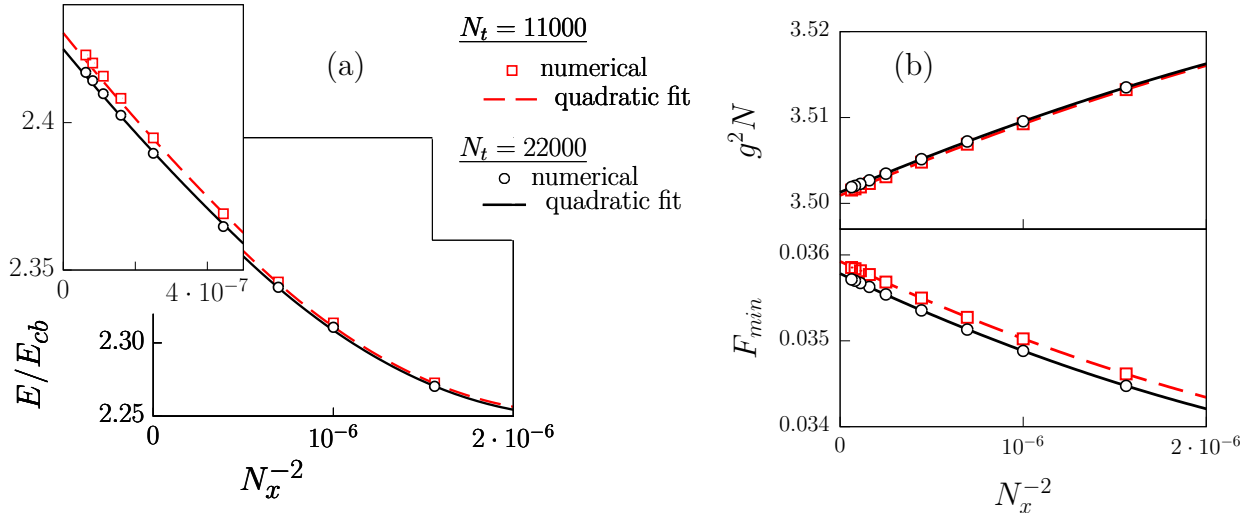


**Figure 7.** Continuum limits  $N_x \rightarrow +\infty$  of the (a) real-time instanton energy  $E$ , (b) its initial particle number  $N$  and suppression exponent  $F_N = F_{min}$ ;  $\theta = 0.199$ . We fit the data points with quadratic functions of  $\delta \equiv N_x^{-2}$  (lines) in the range  $N_x = 800 \div 4000$ .

In Appendix B we demonstrate that any smooth solution has exponential asymptotics,

$$\varepsilon_k \rightarrow \varepsilon_0 e^{-2\omega_k T_*} \quad \text{as} \quad k \rightarrow +\infty, \quad (4.2)$$

where  $T_*$  is a parameter of the solution. Extracting  $a_k$  and  $b_k^*$  from Eq. (4.2) and initial condition (3.3), one finds that the integral in Eq. (3.2) converges at  $|T_{AB} - T| < T_*$  and diverges otherwise. Thus,  $T_*$  is the distance from the optimal contour to the nearest singularity of the solution,  $T_* = |T - \text{Im } t_*|$ .

In Fig. 6b we plot energy distributions  $\varepsilon_k$  for the real-time instanton with  $\theta = 0.199$  at different  $N_x$ . At larger  $N_x$  and  $\omega_k \gg m$  the graphs approach Eq. (4.2) with  $T_* \approx 0.013$ . This indicates that the continuum limit of our numerical solution is a smooth configuration with singularities at finite distances  $T_*$  from the real time axis.

Note that the latter fact is important because our conclusions about existence and properties of the real-time instantons rely on numerical calculations. In Fig. 7 we study the continuum limit in more detail. If  $\phi_{rt}(t, x)$  are smooth configurations, the numerical errors are expected to be polynomials in  $\delta \equiv N_x^{-2} \propto (\Delta x)^2$  and  $N_t^{-2}$  because we use the second-order finite-difference methods. This is indeed the case: lattice values of  $E$ ,  $N$  and  $F_{min}$  (points in Fig. 7) are not sensitive to  $N_t$  and well approximated by quadratic functions of  $\delta$  (lines). At large  $N_x$  all numerical errors are proportional to  $\delta$ , see the inset in Fig. 7a. Once again we conclude that our lattice solutions with  $T = 0$  have well-defined continuum limits.

Numerical results for the minimal suppressions  $F_{min}(N)$  and respective energies  $E_{rt}(N)$  are shown in Fig. 8. Dashed lines in Fig. 8b are the lattice results<sup>17</sup>, while the solid lines represent

<sup>17</sup>In Fig. 8a they are indistinguishable from the continuum limit.



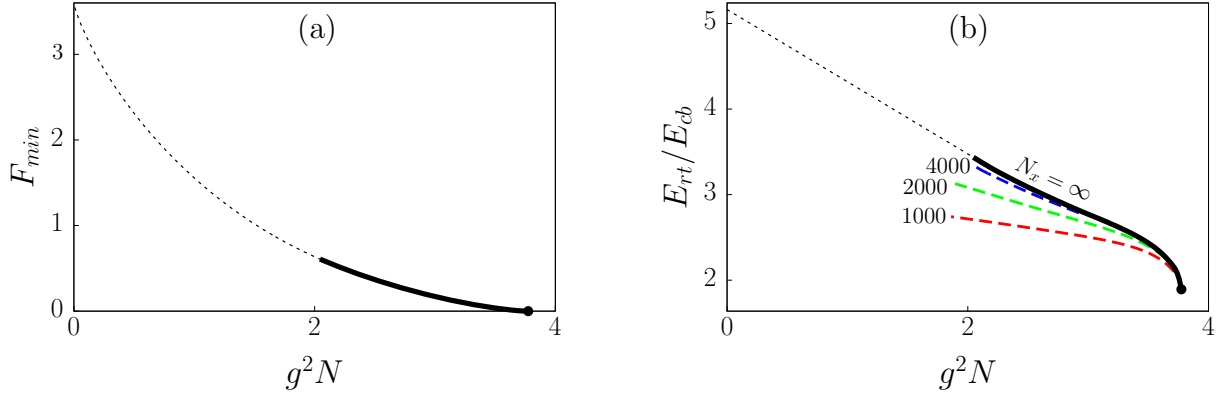


**Figure 8.** (a) Suppression exponent  $F_{min}(N)$  and (b) energy  $E_{rt}(N)$  of the real-time instantons. Dashed lines in Fig. (b) are the lattice results at  $N_t = 11000$  and different  $N_x$  (numbers near the lines). Thick solid lines are obtained by extrapolating results to  $N_x \rightarrow +\infty$ .

continuum limits obtained by quadratic extrapolations in  $\delta = N_x^{-2}$  to  $\delta = 0$ , cf. Fig. 7. Points  $E = E_{rt}$  in Fig. 1c are extracted from Fig. 8. In particular, we obtain results for the few-particle initial states  $g^2 N \ll 1$  by extrapolating  $E_{rt}(N)$  to  $g^2 N = 0$  with linear function, and  $F_{rt}(N)$  by the method described in the end of Sec. 3, see the dotted lines in Fig. 8. The accuracy of our result for  $F_{rt}(0)$  is better than 5%, while extrapolation of energy should be considered as illustrative. In particular, we cannot completely exclude the possibility that  $E_{rt} \rightarrow +\infty$  at  $g^2 N \rightarrow 0$ . Nevertheless, it is likely that the point  $E = E_{rt}$  exists for the few-particle initial states, since it does for the multiparticle ones, cf. Refs. [22, 23].

## 5 Transitions at $E > E_{rt}$

Numerical solutions at  $E > E_{rt}(N)$  look similar to the real-time instantons, cf. Figs. 10a and 6a. But in fact they are fundamentally different: we are going to demonstrate that the solutions above  $E_{rt}$  do not have continuum limits and lead to energy-independent suppression exponent  $F_N(E) = F_{min}(N)$ .

To begin with, we find that the lattice values of the parameter  $T$  monotonously decrease with energy and become negative at  $E > E_{rt}(N)$ , see Fig. 10b. Then Eq. (3.6) implies that the exponent  $F_N(E)$  reaches minimum at  $E = E_{rt}(N)$  and increases at higher energies. The last feature, however, is not expected in continuum models. Indeed, the sum in the definition (3.1) of  $F_N(E)$  runs over all initial states with energy  $E$  and multiplicity  $N$ . These include, in particular, the state where  $N - 1$  particles perform transition at smaller energy  $E_0$  and one spectator particle carries the energy excess  $\Delta E = E - E_0$ , see Fig. 9. The suppression exponent of the last process is  $F_{N-1}(E_0) \approx F_N(E_0)$ , where correction of order  $g^2 \theta \ll 1$  is ignored, cf.

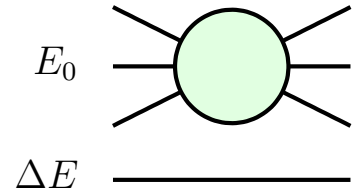


**Figure 9.** Exclusive transition at  $E > E_{rt}(N)$ .



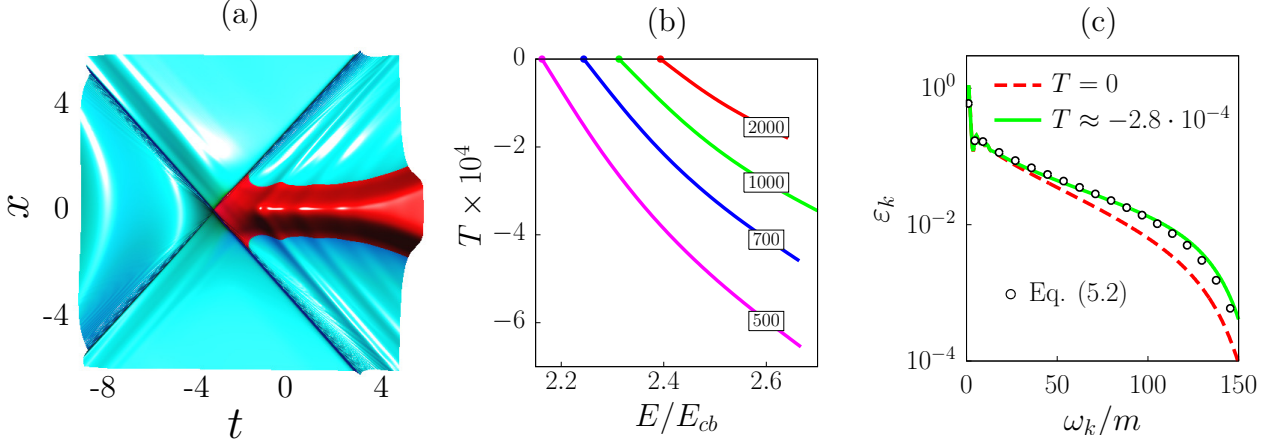


**Figure 10.** (a) Numerical solution  $\phi_s(t, x)$  at  $E \approx 2.6E_{cb} > E_{rt}(N)$ . The other parameters are  $g^2N \approx 3.5$ ,  $T \approx -2.8 \cdot 10^{-4}$ , and  $N_x = 1000$ . (b) Parameter  $T$  in the region  $E > E_{rt}(N)$  for different  $N_x$  (numbers in boxes). (c) Energy distributions for the solution (a) and the real-time instanton with  $N_x = 1000$  from Fig. 6b. In all figures  $\theta = 0.199$  and  $N_t = 11000$ .

Eq. (3.6). Since the inclusive transition is less suppressed than the exclusive one, we conclude that  $F_N(E) \leq F_N(E_0)$ , i.e.  $F_N(E)$  is a non-increasing function of energy.

The above argument suggests that the negative values of  $T \propto -\partial_E F_N$  in Fig. 10b are lattice artifacts and one should be careful with the continuum limit  $\Delta x \rightarrow 0$ . Indeed, Fig. 10c shows that the high-frequency modes of solutions with  $E > E_{rt}(N)$  are enhanced as compared to the case of the real-time instanton and Eq. (4.2). To perform the quantitative comparison, we boldly assume that the semiclassical solutions at  $T < 0$  have the form  $\phi_s(x) = \phi_{rt}(x) + \delta\phi(x)$ , where  $\delta\phi$  consists of high-frequency modes evolving linearly in the real-time instanton background. Ignoring reaction of the latter on  $\delta\phi$ , we write,

$$\delta\phi(x) = \int \frac{dk}{4\pi\omega_k} [\delta c_k e^{-ik \cdot x} + \delta c_k^* e^{ik \cdot x}] . \quad (5.1)$$

This solution is real at  $t \rightarrow +\infty$  because  $\delta c_k$  and  $\delta c_k^*$  are the mutually conjugate constants. One expresses  $\delta c_k$  from the initial condition (3.3):  $\delta c_k = (b_k^{(rt)}\gamma_k - a_k^{(rt)})/(1 - \gamma_k)$ , where  $\gamma_k = e^{-2\omega_k T - \theta}$ . Here and below we mark quantities related to the real-time instanton with “(rt)”, e.g.  $a_k^{(rt)} = e^{-\theta} b_k^{(rt)}$ . We obtain the energy distribution for the solution with  $T < 0$ ,

$$\varepsilon_k \equiv \frac{1}{4\pi} (a_k^{(rt)} + \delta c_k)(b_k^{(rt)*} + \delta c_k^*) = \varepsilon_k^{(rt)} \frac{\sinh^2(\theta/2)}{\sinh^2(\omega_k T + \theta/2)} , \quad (5.2)$$

where  $\varepsilon_k^{(rt)} = a_k^{(rt)} b_k^{(rt)*} / 4\pi$ . Recall that Eq. (5.2) is based on a crude assumption that the solutions with  $E > E_{rt}(N)$  differ from the real-time instantons only in linearly evolving high-frequency modes. Nevertheless, this scaling works well: in Fig. 10c the function (5.2) (points) coincides with the actual energy distribution (solid line). In Appendix B we derive Eq. (5.2) in somewhat different approach.

Distributions (5.2) are qualitatively different at  $T > 0$  and  $T < 0$ . In the former case the high-frequency asymptotics of  $\varepsilon_k$  is consistent with Eq. (4.2) which implies smooth con-

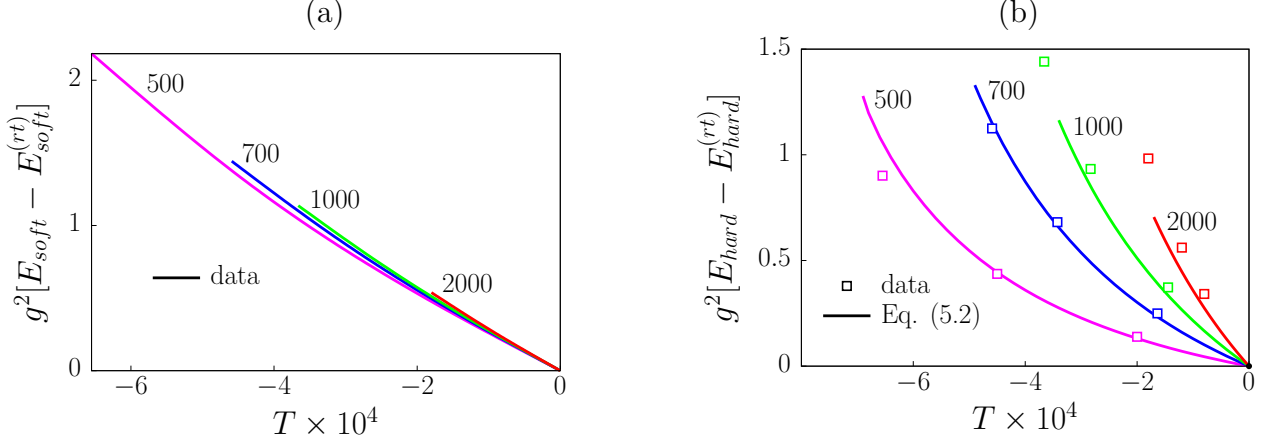


**Figure 11.** Energies of (a) soft and (b) hard modes of solutions at  $E > E_{rt}(N)$  and different  $N_x$  (numbers near the lines);  $\theta = 0.199$ .

tinuum limit. At  $T < 0$ , however, the function (5.2) develops a nonintegrable singularity at  $\omega_k = \omega_* \equiv -\theta/2T$ . Technically, this feature is related to the fact that the linear mode with frequency  $\omega_*$  satisfies reality conditions at  $t \rightarrow \pm\infty$  in Fig. 4a. Solutions can accumulate macroscopic energy in this mode before its amplitude  $\delta c_{k*}/\omega_* \sim \varepsilon_{k*}^{1/2}/\omega_*$  becomes large and linear approximation (5.1) breaks down. Importantly, the latter energy tends to infinity as  $T \rightarrow -0$  or  $\omega_* \rightarrow +\infty$ .

Lattice solutions do not feel the singularity in Eq. (5.2) if the maximal lattice frequency  $\omega_{max} = 2/\Delta x$  is below  $\omega_*$ . If we decrease  $\Delta x$  with constant  $(T, \theta)$ , the value of  $\omega_{max}$  approaches  $\omega_*$  and the solution gains energy. Vice versa, at fixed energy one obtains smaller  $|T|$  at smaller  $\Delta x$ . If Eq. (5.2) is valid up to infinitesimally small  $\Delta x$ , parameter  $T$  approaches zero as  $\Delta x \rightarrow 0$ , so that  $\omega_*$  is kept outside of the lattice frequency range and the energy remains finite. The respective semiclassical solutions arrive at the real-time instanton plus modes with infinitely high frequency and vanishingly small amplitude carrying the energy excess  $E - E_{rt}(N)$ . These solutions do not have smooth continuum limits.

The scaling property of our solutions is best summarized by dividing the total energy into “soft” and “hard” parts, i.e.  $E = E_{soft} + E_{hard}$ , involving modes with  $\omega_k < \omega_\Lambda$  and  $\omega_\Lambda < \omega_k < \omega_{max}$  in Eq. (3.4). In Fig. 11 we plot  $E_{soft}(T)$  and  $E_{hard}(T)$  for  $\omega_\Lambda = 70m$  and several values of  $N_x$ . Predictably,  $E_{soft}$  is not sensitive to  $N_x$ , while  $E_{hard}$  sharply depends on it according to Eq. (5.2) (lines in Fig. 11b). Since the data points in Fig. 11b are well approximated by Eq. (5.2), the value of  $T$  approaches zero as  $N_x \rightarrow +\infty$  at fixed  $E_{hard}$ , so that  $E_{soft} \rightarrow E_{soft}^{(rt)}$  in Fig. 11a.

A remark is in order. Our numerical results show that at high enough  $E - E_{rt}(N)$  the singularity  $\omega_*$  falls below  $\omega_{max}$  and interaction of high-frequency modes becomes important. We find, however, that the above qualitative picture holds even in this case. In particular,  $|T|$  decreases with  $N_x$  at fixed total energy  $E$ , see Fig. 10b. We therefore expect that the respective continuum limit has the same properties: parameter  $T$  vanishes as  $N_x \rightarrow \infty$  and

lattice solutions approach the real-time instanton plus high-frequency modes.

It is important to point out that the lattice solutions lacking smooth continuum limits at  $E > E_{rt}(N)$ , are still capable of describing tunneling transitions in that region. Namely, instead of discretizing the semiclassical equations in Fig. 4a one can start from the lattice path integral for the cross section (3.1). The latter is the ordinary integral over  $N_t \times 2N_x$  variables  $\phi_{ij}$ . At  $g^2 \rightarrow 0$  it is saturated by the semiclassical lattice solutions, and existence of their continuum limits is irrelevant. The overall semiclassical results are reliable if the exponent  $F_N(E)$  itself has a well-defined limit as  $\Delta x \rightarrow 0$ . Then the lattice solutions point at the dominant mechanism of transition.

We have already argued that our lattice solutions with  $E > E_{rt}(N)$  describe processes shown in Fig. 9: they tend to real-time instanton at energy  $E_{rt}(N)$  plus few spectator particles in the form of high-frequency waves carrying the energy excess  $E - E_{rt}(N)$ . The respective suppression exponent is constant because  $T \propto -\partial_E F_N$  approaches zero as  $\Delta x \rightarrow 0$ . We finally conclude that  $F_N(E) = F_{min}(N)$  at energies above  $E_{rt}(N)$ , see Fig. 1c and cf. Refs. [21, 23].

## 6 Stability of perturbative expansion around the real-time instanton

Since the inclusive cross section does not grow exponentially with energy at  $E > E_{rt}$ , one assumes that the terms of its perturbative expansion in  $g^2$  around the real-time instanton are also bounded as  $E \rightarrow +\infty$ . Then one can compute the collision-induced amplitudes and cross sections perturbatively at  $N = 2$  and arbitrary high energies.

To test this property, we directly address the two-particle inclusive cross section of collision-induced false vacuum decay,

$$\sigma(E) = \sum_{\Psi_f} \left| \langle \Psi_f | \hat{U}(t_f, t_i) \hat{a}_{p_2}^\dagger \hat{a}_{p_1}^\dagger | \Psi_0 \rangle \right|^2, \quad (6.1)$$

where  $t_{i,f} \rightarrow \mp\infty$ , the initial state describes two particles with total momentum  $P \equiv p_1 + p_2 = (E, 0)$  in the false vacuum  $\Psi_0$ , each final state  $\Psi_f$  contains an expanding bubble of true vacuum, and we ignore prefactors. If the above expectation is correct, we can extract the cross section (6.1) from the perturbative Green's functions in the backgrounds of the real-time instantons, and corrections to the perturbative calculations will remain small as  $E \rightarrow +\infty$ .

In this Section we compute only the “factorized” contribution to  $\sigma(E)$  which was dominant and responsible for the exponential growth of the inclusive cross section in the Euclidean approach of Sec. 2. We will see that the same contribution is exponentially suppressed if the real-time instanton is used as a background. A consistent perturbative expansion around  $\phi_{rt}(x)$  will be developed in the next Section.

We start from the Green's function (1.4) between the false vacuum  $\Psi_0$  and the dominant final state  $\Psi_{rt}$  of the real-time instanton  $\phi_{rt}(x)$ . Saturating the path integral in Eq. (1.4) with<sup>18</sup>

---

<sup>18</sup>Dependence of our results on parameter  $N$  of the real-time instanton will be discussed in the next Section.

$\phi_{rt}(x - x_0)$ , we find,

$$\mathcal{G}_{rt} = \mathcal{A}_{rt} \int d^2x_0 \Psi_{rt}^*[\phi_{rt}] \phi_{rt}(x_1 - x_0) \dots \phi_{rt}(x_{n+2} - x_0) , \quad (6.2)$$

where<sup>19</sup>

$$\mathcal{A}_{rt} = e^{iS[\phi_{rt}]} \Psi_0[\phi_{rt}] . \quad (6.3)$$

Note that the position  $x_0$  of  $\phi_{rt}$  is not fixed by the semiclassical equations in Fig. 4a. Nevertheless, the final-state wave functional  $\Psi_{rt}[\phi_{rt}]$  depends on  $x_0$  via  $\phi_{rt}(x - x_0)$ .

We use the LSZ reduction formula and turn Eq. (6.2) into the  $2 \rightarrow n + \Psi_{rt}$  amplitude. Considering the initial particles, we trade two of  $\phi$ 's in the integrand for their positive-frequency residues  $b_p^* e^{-ip \cdot x_0}$ , see Eq. (3.2). The case of final-state particles is more involved because at  $t \rightarrow +\infty$  the real-time instanton contains, apart from the outgoing particles, an interacting bubble. To handle this difficulty, we assume that the false vacuum decay occurs in a finite volume  $|x| < L$  with periodic boundary conditions. Then at  $t \rightarrow +\infty$  the bubble fills all space and  $\phi_{rt}(x)$  reduces to waves in the true vacuum,

$$\phi_{rt}(x - x_0) \rightarrow \phi_+ + \int \frac{dk}{4\pi\omega_k^{(+)}} [c_k e^{-ik \cdot (x - x_0)} + c_k^* e^{ik \cdot (x - x_0)}] \quad \text{as} \quad t \rightarrow +\infty , \quad (6.4)$$

where  $k^\mu = (\omega_k^{(+)}, k)$  are the on-shell momenta in the vacuum  $\phi_+$ . The LSZ formula substitutes  $\phi_{rt}(x - x_0)$  with its residue  $c_k e^{ik \cdot x_0}$  for every final-state particle. For clarity below we consider finite  $L$  and do not study the limit  $L \rightarrow +\infty$ .

We obtain,

$$\mathcal{A}'_{2 \rightarrow n + \Psi_{rt}} = \mathcal{A}_{rt} \int d^2x_0 \frac{b_{p_1}^* b_{p_2}^*}{g^{2+n}} c_{k_1} \dots c_{k_n} \Psi_{rt}^*[\phi_{rt}] e^{ix_0 \cdot (k_1 + \dots + k_n - p_1 - p_2)} . \quad (6.5)$$

Here  $p_j$  and  $k_i$  are the momenta of the initial and final particles, the prime of  $\mathcal{A}'$  reminds that only the factorized contribution is considered. Unlike in Sec. 2, we do not explicitly integrate over  $x_0$  because  $\Psi_{rt}$  depends on it in a nontrivial way. Indeed, since  $\phi_{rt}(x)$  is real at  $t \rightarrow +\infty$ , its dominant final state is a coherent one [61][44]: in the interaction representation

$$|\Psi_{rt}\rangle = \exp \left\{ \int dk \frac{c_k \hat{c}_k^\dagger}{4\pi g^2 \omega_k^{(+)}} \right\} |\Psi_+\rangle , \quad (6.6)$$

where we introduced creation operators  $\hat{c}_k^\dagger$  in the true vacuum  $\Psi_+$ . Parameters  $c_k$  of  $\Psi_{rt}$  are precisely the final-state residues  $c_k$  in Eq. (6.4). One can extract dependence of the wave functional  $\Psi_{rt}[\phi_{rt}]$  on  $x_0$  from its transformation properties  $\hat{c}_k^\dagger \rightarrow \hat{c}_k^\dagger e^{-ik \cdot x_0}$  and  $\Psi_+ \rightarrow e^{-it_0 E_+} \Psi_+$  under spacetime shifts  $x \rightarrow x + x_0$ , where  $E_+ = 2LV(\phi_+) < 0$  is the energy of the true vacuum.

---

<sup>19</sup>Recall that  $S$  and  $\Psi_0$  are independent of  $x_0$  in the limit  $t_{i,f} \rightarrow \mp\infty$ , as we drop the terms oscillating with  $t_i$  and  $t_f$ .

The amplitude (6.5) has almost factorized form. In Appendix A we integrate over the phase-space volume and obtain the inclusive cross section,

$$\sigma'(E) = |\mathcal{A}_{rt} b_{p_1} b_{p_2} \Psi_+[\phi_{rt}]|^2 \int d^2\lambda \exp \left\{ iP \cdot \lambda - iE_+ \lambda^0 + \int \frac{dk |c_k|^2}{4\pi g^2 \omega_k^{(+)}} e^{-ik \cdot \lambda} \right\}, \quad (6.7)$$

where  $P \equiv p_1 + p_2 = (E, 0)$ . Equation (6.7) looks similar to Eq. (2.7) of Sec. 2, and yet it is entirely different. First, the initial-state factor  $|b_{p_1} b_{p_2}|^2 \propto e^{-2ET_*}$  decays exponentially with energy because higher momentum transfer from the initial particles to the soft background is less probable, see Eq. (4.2). Second, the final-state contribution is nontrivial because  $\Psi_{rt}$  is not an eigenstate of energy, it absorbs different energies in different cases. Thus, the simple picture of converting all energy into the multiparticle final states with huge phase volume is lost.

Since the exponent in Eq. (6.7) is large, the integral over  $\lambda$  is saturated by the saddle point

$$\lambda_s^\mu = (-2iT', 0) \quad \text{satisfying} \quad E = E_+ + \int dk \frac{|c_k|^2}{4\pi g^2} e^{-2T' \omega_k^{(+)}}. \quad (6.8)$$

At  $E = E_{rt}$  the solution is  $T' = 0$  because the right-hand side of Eq. (6.8) coincides with the final energy of the real-time instanton, cf. Eq. (6.4). At  $E > E_{rt}$  one obtains  $T' < 0$ . Substituting  $\lambda_s$  into Eq. (6.8), we find,

$$\sigma'(E) = |\mathcal{A}_{rt} \Psi_+[\phi_{rt}]|^2 \exp \left\{ 2E(T' - T_*) - 2E_+ T' + \int \frac{dk |c_k|^2 e^{-2T' \omega_k^{(+)}}}{4\pi g^2 \omega_k^{(+)}} \right\} = e^{-F'(E)/g^2}, \quad (6.9)$$

where the suppression exponent is introduced in the second equality.

Equation (6.8) implies that the suppression exponent of  $\sigma'(E)$  grows at  $E > E_{rt}$ ,

$$\frac{dF'}{dE} = 2g^2(T_* - T') > 0. \quad (6.10)$$

In the next Section we will demonstrate that  $F'(E)$  coincides with the true semiclassical exponent  $F(E)$  at  $E = E_{rt}$ . The latter, however, is constant at high energies. Thus, the factorized contribution (6.9) is exponentially subdominant at  $E > E_{rt}$ .

## 7 Perturbative method at high energies

Before considering the dominant contribution, we remark that the perturbative approach of the previous Section is incomplete. Indeed, there is a large family of real-time instantons depending<sup>20</sup> on  $N$  and position  $x_0$ . Every solution from this family has its own dominant final state  $\Psi_{rt}$  which also depends on  $N$  and  $x_0$ , cf. Eq. (6.6).

Our receipt for perturbative evaluation of the collision-induced cross section at  $E > E_{rt}$  (2) and  $N = 2$  is summarized as follows [26]. One starts from the Green's function (1.4) between

---

<sup>20</sup>Recall that we work in the finite- $L$  box which explicitly breaks Lorentz symmetry. Boosted real-time instantons should be taken into account in the infinite-volume limit.

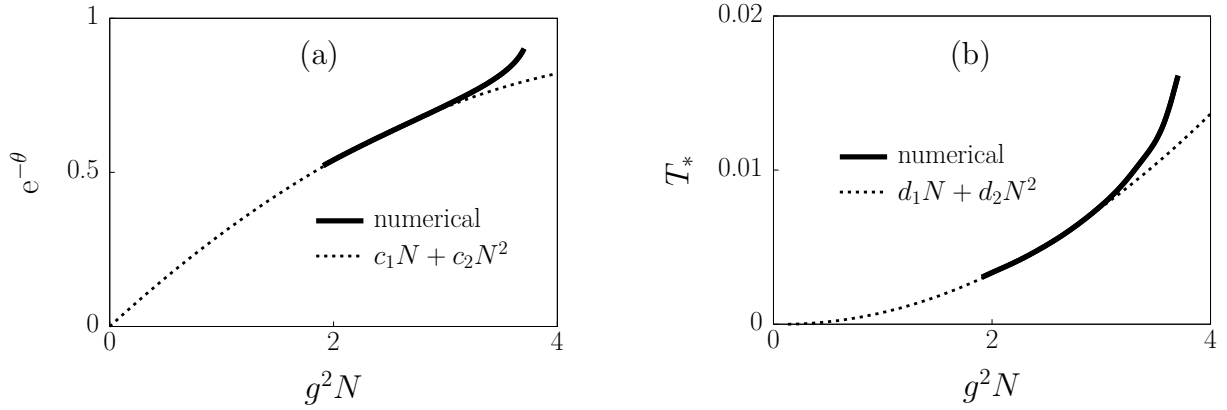


**Figure 12.** Parameters (a)  $e^{-\theta}$  and (b)  $T_*$  of the real-time instanton as functions of  $N$ . Numerical data at  $N_t \times N_x = 11000 \times 3000$  (solid lines) are fitted with quadratic polynomials in  $N$  (dotted lines).

the false vacuum  $\Psi_0$  and the dominant final state  $\Psi_{rt}$  of the real-time instanton  $\phi_{rt}^{(N)}(x - y_0)$ , cf. Eq. (6.6). One evaluates the path integral for the Green's function perturbatively in the background of  $\phi_{rt}$ : substitutes  $\phi(x) = \phi_{rt}^{(N)}(x - x_0) + g\delta\phi(x)$  and expands the integrand in  $g\delta\phi$ . Integral over the would-be flat direction  $x_0 \neq y_0$  remains in the Green's function, cf. Eq. (6.2). One finally extracts the perturbative amplitudes  $\mathcal{A}_{2 \rightarrow n + \Psi_{rt}}$  from the LSZ formula, turns them into the inclusive cross section with the machinery of Appendix A, and takes the limit  $N \rightarrow 0$ . The result is a perturbative expansion for  $\sigma(E)$  which, as we are going to argue, is applicable at arbitrary high energies.

Let us explain the role of the artificial parameter  $N$  in the above procedure. On the one hand, the limit  $N \rightarrow 0$  formally corresponds to vacuum initial state of the real-time instanton. Indeed, at  $\theta \rightarrow +\infty$  one simultaneously obtains Feynman initial condition  $a_k \rightarrow 0$  for  $\phi_{rt}^{(N)}$  and  $N \rightarrow 0$ , see Eqs. (3.3) and (3.4). Thus, the real-time instanton with  $N = 0$  and  $x_0 = y_0$  is the formal saddle-point configuration<sup>21</sup> for the path integral (1.4), and the perturbative series around it constitute the ordinary saddle-point expansion. On the other hand, the energy  $E_{rt}(N)$  of the real-time instanton corresponds to  $\partial_E F_N = 0$  and stays nonzero in the limit  $N \rightarrow 0$ , cf. Fig. 8b. This means that  $\phi_{rt}^{(N)}$  is singular at  $N = 0$  because its typical frequencies  $\omega_k \sim E/N$  are infinite. We therefore develop perturbative expansion around the smooth configurations with  $N > 0$  and send  $N \rightarrow 0$  in the end of calculations.

In Fig. 12 we plot parameter  $e^{-\theta}$  of the real-time instanton and distance  $T_*$  to its closest singularity as functions of  $N$ . Numerical data (solid lines) are well fitted by quadratic polynomials with zeros at  $N = 0$  (dashed lines). The graphs support our expectation that as  $N \rightarrow 0$ , the real-time instanton  $\phi_{rt}^{(N)}$  tends to a singular configuration with vacuum initial conditions.

Expanding the integrand of Eq. (1.4) in  $g\delta\phi$ , we obtain Feynman rules involving points,

<sup>21</sup>Recall that  $\phi_{rt}^{(N)}$  extremizes the classical action and, by construction of  $\Psi_{rt}$ , saturates the integral with the final state at  $x_0 = y_0$ .

propagators and vertices,

$$x \bullet = \frac{\phi_{rt}}{g} \Big|_{x-x_0}, \quad x \text{---} y = \langle \delta\phi(x) \delta\phi(y) \rangle_{rt}, \quad \text{---} x \text{---} = g^{m-2} V^{(m)}(\phi_{rt}) \Big|_{x-x_0}, \quad (7.1)$$

which explicitly depend on  $N$  and  $x_0$ . At nonzero  $N$  or  $x_0 \neq y_0$  one also obtains the tadpoles i.e. terms in action proportional to  $\delta\phi$ . The tadpoles related to the initial state vanish as  $N \rightarrow 0$  and we do not consider them in what follows. The final-state tadpoles are related to the fact that  $\Psi_{rt}$  is the dominant final state for the configuration  $\phi_{rt}(x - y_0)$  which is different from our background  $\phi_{rt}(x - x_0)$ . We will discuss them in the end of this Section. Since the elements in Eq. (7.1) explicitly depend on  $x$ , energy and momentum are not conserved along the lines and in the vertices. Rather, the Feynman rules in momentum space involve structure functions depending on momentum  $Q$  transferred to the background. We will see shortly that the real-time instanton consumes total energy  $Q^0 \approx E_{rt}$  from the initial particles.

At zeroth order of perturbative expansion one uses  $\phi(x) = \phi_{rt}^{(N)}(x - x_0)$  in Eq. (1.4) and obtains the diagram in Fig. 13a. Extracting the cross section and summing over the final states, one arrives at the contribution (6.9) which is exponentially subdominant. Indeed, we argued in Eq. (6.10) that the suppression exponent  $F'(E)$  of this contribution grows with energy at  $E > E_{rt}$ . Besides, at  $E = E_{rt}$  and  $N \rightarrow 0$  we have  $T' = T_* = 0$  and therefore

$$F'(E_{rt}) = 2g^2 \text{Im } S[\phi_{rt}] - g^2 \ln |\Psi_0|^2 - g^2 \ln |\Psi_+|^2 - \int \frac{dk |c_k|^2}{4\pi\omega_k^{(+)}} = F(E_{rt}) + O(N). \quad (7.2)$$

Here we used Eqs. (6.3) and (3.5), vacuum wave functionals

$$\Psi_0[\phi] = \exp \left\{ - \int \frac{dk \omega_k}{4\pi g^2} \phi(k) \phi(-k) \right\}_{t_i}$$

and  $\Psi_+[\phi]$ , spatial Fourier transform  $\phi(k)$  of configuration  $\phi$ , and representations (3.2), (6.4) of the real-time instanton<sup>22</sup>. Since the dominant exponent  $F(E)$  is constant at high energies, we repeat that  $F'(E) > F(E)$  at  $E > E_{rt}$ , i.e. the factorized diagram in Fig. 13a is negligible.<sup>23</sup>

The dominant diagram at  $E > E_{rt}$  is shown in Fig. 13b. It describes propagation of two initial particles which transfer momentum  $Q = q_1 + q_2$  to the background. The respective transition amplitude is<sup>24</sup>,

$$\mathcal{A}_{2 \rightarrow n + \Psi_{rt}} = \mathcal{A}_{rt} n(n-1) \int d^2 x_0 D_{p_1, k_1} D_{p_2, k_2} \frac{c_{k_3} \cdots c_{k_n}}{g^{n-2}} \Psi_{rt}^*[\phi_{rt}] e^{ix_0 \cdot (k_3 + \cdots + k_n - q_1 - q_2)}, \quad (7.3)$$

<sup>22</sup>Recall also that  $F_N(E) = F(E) - g^2 \theta N + O(N)$  as we argued in the end of Sec. 3.

<sup>23</sup>One finds that as  $L \rightarrow \infty$ , the energy of the true vacuum becomes infinite and therefore  $T' \rightarrow 0$ . Thus, in the infinite-volume limit the contribution (6.9) becomes comparable to the dominant one.

<sup>24</sup>Symmetrization with respect to permutations of  $k_1, \dots, k_n$  is assumed.



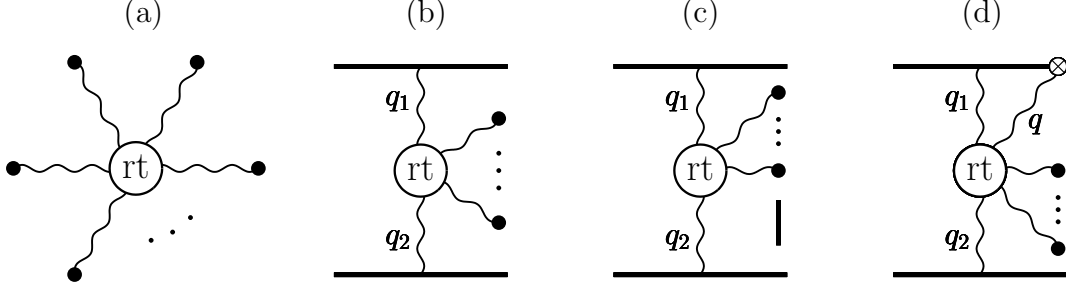


**Figure 13.** Diagrams for perturbative expansion around the real-time instanton.

cf. Eq. (6.5). Here  $q_i \equiv p_i - k_i$  and  $D_{p,k} \cdot e^{-iq \cdot x_0}$  is the double residue<sup>25</sup> of the propagator  $\langle \delta\phi \delta\phi \rangle_{rt}$ . In Appendix A we convert the amplitude into inclusive cross section,

$$\sigma(E) = |\mathcal{A}_{rt} \Psi_+[\phi_{rt}]|^2 \int \frac{dk_1 dk_2}{32\pi^2 \omega_{k_1}^{(+)} \omega_{k_2}^{(+)}} |D_{p_1, k_1} D_{p_2, k_2} + D_{p_1, k_2} D_{p_2, k_1}|^2 \times \int d^2\lambda \exp \left\{ iQ \cdot \lambda - iE_+ \lambda^0 + \int \frac{dk |c_k|^2}{4\pi g^2 \omega_k^{(+)}} e^{-ik \cdot \lambda} \right\}, \quad (7.4)$$

where  $\lambda \equiv y_0 - x_0$  and we omit trivial prefactors. The first line in this expression is the naive Feynman diagram in the background of the real-time instanton. The factor in the second line is related to the nontrivial final state of the background process. It is the same as in Eq. (6.7). In Sec. 6 we demonstrated that this factor is sharply peaked around  $Q^\mu = (E_{rt}, 0)$  with fluctuations of order  $\Delta Q \sim gE_{rt}$ .

With exponential precision,

$$\sigma(E) = e^{-F(E_{rt})/g^2} \quad \text{at} \quad E > E_{rt},$$

where Eq. (7.2) was exploited. We thus obtained constant suppression exponent  $F = F(E_{rt})$  at  $E > E_{rt}$  which was deduced in Sec. 5 on the basis of sophisticated numerical analysis. Note that our perturbative method can be easily extended to calculate prefactor: one just has to estimate the energy-independent saddle-point determinant in the Green's function (1.4) and collect few simple prefactors in the above calculations.

The first perturbative correction to the dominant contribution is shown in Fig. 13c. It involves the same relative factor  $g^2 n^2$  as in the low-energy calculation of Sec. 2. This time, however, the number  $n$  of additional particles is relatively small and does not grow with collision energy  $E$ . Indeed, any energy transfer to the background above  $Q = E_{rt}$  is cut off by the final-state factor. This means that  $n \sim |Q - E_{rt}|/m \sim g^{-1}$ , and the diagram in Fig. 13c is of the same order as the dominant one. Importantly, it does not grow with energy. Resummation of these disconnected diagrams [48, 49] leaves us with corrections involving vertices which are suppressed by the true expansion parameter  $g$ .

<sup>25</sup>Related to the Bogolyubov coefficients in the nontrivial background  $\phi_{rt}$ .

Let us finally discuss the tadpoles. We saw that the parameter  $y_0$  of  $\Psi_{rt}$  does not coincide with the position  $x_0$  of the background solution: the integral over the difference  $\lambda \equiv y_0 - x_0$  enters Eq. (7.4). Thus,  $\phi_{rt}(x - x_0)$  is not the true saddle-point configuration of the integral (1.4), and perturbative expansion around it starts from the linear term in  $\delta\phi$ . We obtain the tadpole

$$\text{---} \bigcirc_{\text{rt}}^q = \frac{c_q^* e^{-iq \cdot x_0}}{4\pi g \omega_k^{(+)}} (e^{-iq \cdot \lambda} - 1) \quad (7.5)$$

which should be integrated over  $q$  with the final-state residue of the propagator. Apart from the additional integration, this tadpole is similar to the final on-shell particle in the amplitude. One may think that the dominant contribution includes diagrams with the tadpoles attached to the hard propagators, e.g. Fig. 13d. However, all momentum  $p_1 = q_1 + q$  of the propagator with the tadpole is transferred to the real-time instanton. Indeed, Eq. (7.5) is proportional to the exponent  $e^{-iq \cdot x_0}$  which accumulates transferred momentum in the amplitude, cf. Eq. (7.3). Then the total transferred energy in the process of Fig. 13d is higher than  $E_{rt}$  and the respective contribution to the cross section is exponentially small.

We see that the tadpoles infest only the final-state propagators in Fig. 13c and subdominant diagrams. Note that the element (7.5) is  $O(g^0)$  at best. Indeed, at small  $q$  the bracket in Eq. (7.5) is proportional to  $g$  because  $\lambda \sim g$  at  $E \approx E_{rt}$ . At  $q \sim m/g$  the tadpole is suppressed by the factor  $c_q^*/\omega_q^{(+)}$  which vanishes at high  $q$  because the energy of the real-time instanton is finite. Thus, the tadpoles also do not break the perturbative expansion.

We conclude that the perturbative expansion around the real-time instanton is reliable at arbitrarily high energies.

## 8 Summary and discussion

In this paper we studied collision-induced tunneling in field theory. We paid special attention to the case of  $N = 2$  colliding particles with high total energy  $E$ . As a playground we considered induced false vacuum decay in  $(1 + 1)$  dimensions. We demonstrated that the suppression exponent  $F_N(E)$  of this process decreases with energy, reaches minimum  $F = F_{min}(N)$  at  $E = E_{rt}(N)$  and remains constant at higher energies.

Our methods rely on existence of the real-time instantons — a special class of semiclassical solutions describing inclusive collision-induced transitions from the initial states with  $N$  particles and arbitrary energies. The minimal suppression  $F_{min}(N)$  and threshold energy  $E_{rt}(N)$  are computed as functionals on these solutions. Real-time instantons were first observed in the toy model of Ref. [23]. We numerically obtained them in the case of  $(1 + 1)$ -dimensional false vacuum decay. We expect that these solutions exist for other collision-induced tunneling processes. One can verify this expectation on a case-to-case basis by solving the respective semiclassical boundary value problem in a given model.

Importantly, we argue on general grounds that the real-time instantons are complex solutions evolving in real time (hence the title). This property is very unusual for the semiclassical

solutions related to exponentially suppressed transitions, it leads to far-reaching consequences. We find that scattering of high-energy quantum particles in the backgrounds of the real-time instantons resembles scattering in vacuum because energy exchange between the particles and the soft background occurs with exponentially small probability. This situation is radically different from that at low energies where Euclidean semiclassical solutions recycle any additional energy into exponentially large probability factors. Starting from the real-time instantons, we develop a perturbative description of the collision-induced processes at  $N = 2$  and  $E > E_{rt}(2)$ . We demonstrate that this description remains valid at arbitrary high energies. It shows that the suppression exponent  $F(E) \equiv F_2(E)$  is constant at  $E > E_{rt}(2)$ . Besides, the collision-induced transitions themselves involve transfer of fixed energy  $E_{rt}(2)$  from the two colliding particles to the soft background; the energy excess  $E - E_{rt}(2)$  remains in the initial particles till the end of the process. Note that our perturbative methods can be easily generalized for calculation of prefactors or exclusive cross sections.

We conclude that the real-time instantons, if exist for a given collision-induced process, provide powerful perturbative framework and guarantee constant suppression exponent  $F(E) = F_{min}(2)$  of this process at energies above a certain threshold  $E_{rt}(2)$ .

## Acknowledgments

We are grateful to S.M. Sibiryakov and F.L. Bezrukov for motivation and to V.A. Rubakov [62] for criticism. This work is supported by the RSCF grant 14-22-00161. D.L. thanks EPFL for hospitality.

## A Multiparticle cross sections

In this Appendix we evaluate inclusive cross sections for the amplitudes considered in the main body of the paper. We start from the factorized  $2 \rightarrow n$  amplitude

$$\mathcal{A}_{2 \rightarrow n} = \frac{\mathcal{A}_0}{g^n} c_{k_1} \dots c_{k_n} . \quad (\text{A.1})$$

Here  $\mathcal{A}_0$  and  $g$  are constants,  $k_i$  are momenta of particles in the final state. The cross section of inclusive transition to the  $n$ -particle final states is obtained by integrating over the phase space volume  $\Pi_n$ ,

$$\begin{aligned} \sigma_n(P) &= \int |\mathcal{A}_{2 \rightarrow n}|^2 d\Pi_n(P) \\ &= \frac{|\mathcal{A}_0|^2}{n!} \int \frac{dk_1 |c_{k_1}|^2}{4\pi g^2 \omega_{k_1}} \dots \int \frac{dk_n |c_{k_n}|^2}{4\pi g^2 \omega_{k_n}} (2\pi)^2 \delta^{(2)}(k_1 + \dots + k_n - P) , \end{aligned}$$

where we ignored the initial-state factor, introduced the total initial momentum  $P_\mu$  and on-shell frequencies  $\omega_k^2 = k^2 + m^2$ . We use Fourier representation of the  $\delta$ -function and find,

$$\sigma_n(P) = \frac{|\mathcal{A}_0|^2}{n!} \int d^2\lambda [f(\lambda)]^n e^{iP \cdot \lambda} , \quad \text{where} \quad f(\lambda) = \int \frac{dk |c_k|^2}{4\pi g^2 \omega_k} e^{-ik \cdot \lambda} . \quad (\text{A.2})$$

If  $c_k = c_b$  does not depend on  $k$ ,

$$f(\lambda) = \frac{|c_b|^2}{2\pi g^2} K_0(m\sqrt{-\lambda^2 + i\epsilon\lambda^0}) .$$

Equation (A.2) shows that  $\lambda$  is a typical Compton wavelength of the final particles,  $\lambda \sim k^{-1}$ . Summing up the  $n$ -particle contributions (A.2), we obtain Eq. (2.7) of Sec. 2.

In Sec. 6 we consider the factorized amplitude (6.5) of the process  $2 \rightarrow n + \Psi_{rt}$ . To simplify summation over final states in the inclusive cross section, we extract the ordinary  $2 \rightarrow n + m$  amplitudes. Namely, expanding the exponent in Eq. (6.6), we obtain

$$\mathcal{A}'_{2 \rightarrow n + \Psi_{rt}} = \sum_{m=0}^{\infty} \frac{1}{m!} \int \frac{dk_{n+1} c_{k_{n+1}}^*}{4\pi g \omega_{k_{n+1}}^{(+)}} \cdots \int \frac{dk_{n+m} c_{k_{n+m}}^*}{4\pi g \omega_{k_{n+m}}^{(+)}} \mathcal{A}'_{2 \rightarrow n+m} (2\pi)^2 \delta^{(2)}(P - P_f) . \quad (\text{A.3})$$

where  $P_f$  is the total momentum of the  $(n+m)$ -particle final state. Next, we compare the amplitude (6.5) with Eq. (A.3). Substituting  $\phi = \phi_{rt}$  into the wave functional  $\Psi_d[\phi]$  of a coherent state [25] with parameters  $d_k e^{-i\omega_k t_f}$ , we find,

$$\Psi_d[\phi_{rt}] \equiv \langle \phi | \Psi_d \rangle = \exp \left\{ \int dk \frac{d_k c_k^* e^{-ik \cdot x_0}}{4\pi g^2 \omega_k^{(+)}} \right\} e^{-iE_+ t_0} \Psi_+[\phi_{rt}] , \quad (\text{A.4})$$

where we extracted dependence on  $x_0$  as explained in Sec. 6, used the form (6.4) of  $\phi_{rt}$ , took the limit  $t_f \rightarrow +\infty \cdot e^{-i\epsilon}$  and introduced wave functional  $\Psi_+$  of the true vacuum. The final state  $\Psi_{rt}$  in Sec. 6 has  $d_k = c_k$ , cf. Eq. (6.6). Expanding the exponent in Eq. (A.4) and substituting the series into Eq. (6.5), we find,

$$\begin{aligned} \mathcal{A}'_{2 \rightarrow n + \Psi_{rt}} &= \sum_{m=0}^{\infty} \frac{1}{m!} \int \frac{dk_{n+1} |c_{k_{n+1}}|^2}{4\pi g^2 \omega_{k_{n+1}}^{(+)}} \cdots \int \frac{dk_{n+m} |c_{k_{n+m}}|^2}{4\pi g^2 \omega_{k_{n+m}}^{(+)}} \times \\ &\quad \times \frac{\mathcal{A}_0}{g^n} c_{k_1} \cdots c_{k_n} (2\pi)^2 \delta^{(2)}(P - P_f) . \end{aligned} \quad (\text{A.5})$$

Here we evaluated the integral over  $x_0$  and introduced  $\mathcal{A}_0 = \mathcal{A}_{rt} \Psi_+^*[\phi_{rt}] b_{p_1}^* b_{p_2}^* / g^2$ . Comparing Eqs. (A.3) and (A.5), one finds that the amplitudes  $\mathcal{A}'_{2 \rightarrow n+m}$  have the form (A.1). We finally obtain the inclusive cross section (6.7) by summing up the  $n$ -particle ones in Eq. (A.2).

To process the dominant amplitude (7.3) of Sec. 7, we do the opposite to the above, i.e. combine the final states into the coherent states  $\Psi_d$  with parameters  $d_k \equiv c_k e^{ik \cdot y_0} + \delta c_k$ , where  $c_k e^{ik \cdot y_0}$  are the parameters of  $\Psi_{rt}$  and  $\delta c_k$  are arbitrary. We find,

$$\begin{aligned} \mathcal{A}_{2 \rightarrow \Psi_d} &= \sum_{n=0}^{\infty} \frac{1}{n!} \int \frac{dk_1 \delta c_{k_1}^*}{4\pi g \omega_{k_1}^{(+)}} \cdots \int \frac{dk_n \delta c_{k_n}^*}{4\pi g \omega_{k_n}^{(+)}} \mathcal{A}_{2 \rightarrow n + \Psi_f^{rt}} \\ &= \mathcal{A}_{rt} \int d^2 x_0 \Psi_d^*[\phi_{rt}] \int \frac{dk_1 dk_2 \delta c_{k_1}^* \delta c_{k_2}^*}{16\pi^2 g^2 \omega_{k_1}^{(+)} \omega_{k_2}^{(+)}} D_{p_1, k_1} D_{p_2, k_2} e^{-ix_0 \cdot (q_1 + q_2)} , \end{aligned} \quad (\text{A.6})$$

In the first line of this expression we expanded  $\Psi_d$  in  $\delta c$  using Eq. (6.6), in the second substituted Eq. (7.3) and introduced wave functional  $\Psi_d[\phi_{rt}]$ , Eq. (A.4).

Now, we evaluate the inclusive cross section

$$\sigma(E) = \frac{1}{V^{(2)}} \int \mathcal{D}d' \mathcal{D}d^* \mathcal{A}_{2 \rightarrow \Psi_d} \mathcal{A}_{2 \rightarrow \Psi_{d'}}^* \exp \left\{ - \int \frac{dk d'_k d_k^*}{4\pi g^2 \omega_k^{(+)}} \right\}, \quad (\text{A.7})$$

where  $V^{(2)}$  is the spacetime volume. First, we note that the amplitude (A.7) depends on the arbitrary parameter  $y_0$ . This is the freedom of choosing the background for expansion, it disappears after resummation of perturbative series. We fix the freedom requiring

$$y_0 = x'_0, \quad y'_0 = x_0, \quad (\text{A.8})$$

where  $y'_0$  and  $x'_0$  come from the complex conjugate amplitude (A.6) in the integral for the inclusive cross section. Second, the parameters  $\delta c_k^*$  in the prefactor can be obtained by varying the exponent  $\exp\{\int dk \alpha_k \delta c_k^* / (4\pi g^2 \omega_k^{(+)})\}$  with respect to  $\alpha$  at  $\alpha = 0$ . The integral in Eq. (A.7) therefore can be evaluated using the functional

$$\begin{aligned} \Pi[\alpha, \alpha'^*] &= \int \mathcal{D}\delta c' \mathcal{D}\delta c^* \Psi_d^*[\phi_{rt}] \Psi_{d'}[\phi_{rt}] \exp \left[ \int \frac{dk}{4\pi g^2 \omega_k^{(+)}} (\alpha_k \delta c_k^* + \alpha'_k \delta c'_k - d'_k d_k^*) \right] \\ &= e^{-iE+\lambda^0} |\Psi_+[\phi_{rt}]|^2 \exp \left[ \int \frac{dk}{4\pi g^2 \omega_k^{(+)}} (\alpha_k \alpha'_k + |c_k|^2 e^{-ik \cdot \lambda}) \right], \end{aligned} \quad (\text{A.9})$$

where we denoted  $d'_k \equiv c_k e^{ik \cdot y'_0} + \delta c'_k$ , substituted Eq. (A.4), evaluated the integrals over  $\delta c^*$ ,  $\delta c'$  and denoted  $\lambda \equiv y_0 - x_0 = x'_0 - x_0$ . We see that variations over  $\alpha_k$  and  $\alpha'_k$  give contraction rule for the final-state variables  $\overline{\delta c_{k_1}} \delta c_{k_2}^* = 4\pi g^2 \omega_k^{(+)} \delta(k_1 - k_2)$ .

Substituting Eqs. (A.6) and (A.9) into Eq. (A.7), one obtains the inclusive cross section (7.4) containing the integral over  $\lambda = x'_0 - x_0$ ; integration with respect to  $(x_0 + x'_0)/2$  gives the two-volume  $V^{(2)}$  which is canceled in Eq. (A.7).

## B High-frequency tail of the semiclassical solution

Let us evaluate high-frequency asymptotics of the saddle-point solution  $\phi_s(x)$ . To this end we represent  $\phi_s(x) = \phi_0(x) + \delta\phi(x)$  as a sum of soft nonlinear background  $\phi_0$  and high-frequency part  $\delta\phi \ll \phi_0$  evolving on top of it. Functions  $\phi_0$  and  $\delta\phi$  contain modes with  $k < \Lambda$  and  $k > \Lambda$ , respectively. One rewrites the field equation as

$$\square \delta\phi(x) = J(x), \quad (\text{B.1})$$

where  $J$  is a contribution of  $\phi_0$  and  $\delta\phi$  is ignored in potential terms. We solve Eq. (B.1),

$$\delta\phi(x) = - \int \frac{d^2 k}{(2\pi)^2} \frac{J(k) e^{-ik \cdot x}}{k^2 - i\epsilon k^0} + \int_{k > \Lambda} \frac{dk}{4\pi \omega_k} [c_k e^{-ik \cdot x} + c_k^* e^{ik \cdot x}], \quad (\text{B.2})$$

using the two-dimensional Fourier image of the source  $J(k)$  and arbitrary on-shell waves in the second term with  $k^\mu = (\omega_k, k)$  and  $\omega_k = |k|$ . The solution (B.2) is real as  $t \rightarrow +\infty$  in accordance with Fig. 4a. In the infinite past, i.e.  $t \rightarrow iT - \infty$ , Eq. (B.2) takes the form (3.2) with

$$a_k = c_k + J_k^- , \quad b_k^* = c_k^* + J_k^+ , \quad \text{and} \quad J_k^\pm \equiv \pm i J(\mp k) \Big|_{k^0 = \omega_k} . \quad (\text{B.3})$$

We finally solve the initial condition (3.3) and obtain,

$$c_k = \frac{\gamma_k (J_k^+)^* - J_k^-}{1 - \gamma_k} , \quad \gamma_k \equiv e^{-2\omega_k T - \theta} . \quad (\text{B.4})$$

Note that Eq. (B.1) and its solution (B.2), (B.4) are valid only at  $k > \Lambda \gg m$ .

One notices that the sources  $J_k^\pm$  are exponentially sensitive to  $k$ . Indeed, the  $t$ -contours in the Fourier transforms

$$J_k^\pm = \pm i \int d^2 x J(x) e^{\mp i k \cdot x} \Big|_{k^0 = \omega_k} \quad (\text{B.5})$$

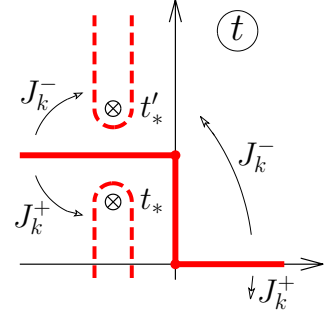
can be deformed into the upper and lower parts of the complex time plane until they hit the singularities  $t_*$  and  $t'_*$  of the solution<sup>26</sup>, see Fig. 14. At large  $k$  the integrals are saturated near the singularities, and

$$J_k^+ \sim J_0^+ e^{-i\omega_k t_*} , \quad J_k^- \sim J_0^- e^{i\omega_k t'_*} \quad (\text{B.6})$$

where  $J_0^\pm$  are constants.

We finally compute the energy of the initial particles with momentum  $k$  in Eq. (3.4) using Eqs. (B.3), (B.4),

$$\varepsilon_k \equiv \frac{a_k b_k^*}{4\pi} = \frac{|(J_k^+)^* - J_k^-|^2}{16\pi \sinh^2(\omega_k T + \theta/2)} , \quad (\text{B.7})$$



Estimating the largest term in the nominator by Eq. (B.6), one obtains the high-frequency asymptotic (4.2) with  $T_* = T + \min(-\text{Im } t_*, \text{Im } t'_*)$ . Equation (B.7) obeys<sup>27</sup> the rescaling property (5.2) of Sec. 5.

## References

- [1] A. A. Belavin, A. M. Polyakov, A. S. Schwartz and Y. S. Tyupkin, *Pseudoparticle Solutions of the Yang-Mills Equations*, *Phys. Lett. B* **59** (1975) 85.
- [2] G. 't Hooft, *Computation of the Quantum Effects Due to a Four-Dimensional Pseudoparticle*, *Phys. Rev. D* **14** (1976) 3432 [*Erratum-ibid. D* **18** (1978) 2199].
- [3] V. A. Rubakov and M. E. Shaposhnikov, *Electroweak baryon number nonconservation in the early universe and in high-energy collisions*, *Phys. Usp.* **39** (1996) 461 [*Usp. Fiz. Nauk* **166** (1996) 493] [[hep-ph/9603208](#)].

<sup>26</sup>Recall that  $J(x)$  is related to  $\phi_0(x)$ .

<sup>27</sup>In this case the soft background  $\phi_0$  and related sources  $J_k^\pm$  are almost independent of  $T$ .

- [4] I. V. Krive and A. D. Linde, *On the Vacuum Stability Problem in Gauge Theories*, *Nucl. Phys. B* **117** (1976) 265.
- [5] N. V. Krasnikov, *Restriction of the Fermion Mass in Gauge Theories of Weak and Electromagnetic Interactions*, *Yad. Fiz.* **28** (1978) 549.
- [6] G. Degrassi, S. Di Vita, J. Elias-Miro, J.R. Espinosa, G.F. Giudice, G. Isidori and A. Strumia, *Higgs mass and vacuum stability in the Standard Model at NNLO*, *JHEP* **1208** (2012) 098 [[1205.6497](#)].
- [7] D. Buttazzo, G. Degrassi, P.P. Giardino, G.F. Giudice, F. Sala, A. Salvio and A. Strumia, *Investigating the near-criticality of the Higgs boson*, *JHEP* **1312** (2013) 089 [[1307.3536](#)].
- [8] F. Bezrukov and M. Shaposhnikov, *Why should we care about the top quark Yukawa coupling?*, arXiv:1411.1923.
- [9] A. Ringwald, *High-Energy Breakdown of Perturbation Theory in the Electroweak Instanton Sector*, *Nucl. Phys. B* **330** (1990) 1.
- [10] O. Espinosa, *High-Energy Behavior of Baryon and Lepton Number Violating Scattering Amplitudes and Breakdown of Unitarity in the Standard Model*, *Nucl. Phys. B* **343** (1990) 310.
- [11] M. P. Mattis, *The Riddle of high-energy baryon number violation*, *Phys. Rept.* **214** (1992) 159.
- [12] I.Y. Kobzarev, L.B. Okun and M.B. Voloshin, *Bubbles in Metastable Vacuum*, *Sov. J. Nucl. Phys.* **20** (1975) 644 [*Yad. Fiz.* **20** (1974) 1229].
- [13] M. Stone, *Semiclassical Methods for Unstable States*, *Phys. Lett. B* **67** (1977) 186.
- [14] S.R. Coleman, *The Fate of the False Vacuum. 1. Semiclassical Theory*, *Phys. Rev. D* **15** (1977) 2929 [*Erratum-ibid. D* **16** (1977) 1248].
- [15] S. R. Coleman, *The Uses of Instantons*, *Subnucl. Ser.* **15** (1979) 805.
- [16] N. S. Manton, *Topology in the Weinberg-Salam Theory*, *Phys. Rev. D* **28** (1983) 2019.
- [17] F. R. Klinkhamer and N. S. Manton, *A Saddle Point Solution in the Weinberg-Salam Theory*, *Phys. Rev. D* **30** (1984) 2212.
- [18] V. I. Zakharov, *Unitarity constraints on multiparticle weak production*, *Nucl. Phys. B* **353** (1991) 683.
- [19] V. I. Zakharov, *High-energy production of scalar bosons in weak coupling theories*, *Phys. Rev. Lett.* **67** (1991) 3650.
- [20] M. Maggiore and M. A. Shifman, *Nonperturbative processes at high-energies in weakly coupled theories: Multi-instantons set an early limit*, *Nucl. Phys. B* **371** (1992) 177.
- [21] M. B. Voloshin, *Catalyzed decay of false vacuum in four dimensions*, *Phys. Rev. D* **49** (1994) 2014 [[hep-ph/9309237](#)].
- [22] D. G. Levkov and S. M. Sibiryakov, *Induced tunneling in QFT: Soliton creation in collisions of highly energetic particles*, *Phys. Rev. D* **71** (2005) 025001 [[hep-th/0410198](#)].
- [23] D. Levkov and S. Sibiryakov, *Real-time instantons and suppression of collision-induced*



- tunneling, *JETP Lett.* **81** (2005) 53 [*Pisma Zh. Eksp. Teor. Fiz.* **81** (2005) 60] [[hep-th/0412253](#)].
- [24] G. Veneziano, *Bound on reliable one instanton cross-sections*, *Mod. Phys. Lett. A* **7** (1992) 1661.
  - [25] P. G. Tinyakov, *Instanton-like transitions in high-energy collisions*, *Int. J. Mod. Phys. A* **8** (1993) 1823.
  - [26] V.A. Rubakov, private communication.
  - [27] S. Yu. Khlebnikov, *Semiclassical approach to multiparticle production*, *Phys. Lett. B* **282** (1992) 459.
  - [28] D. Diakonov and V. Petrov, *Nonperturbative isotropic multiparticle production in Yang–Mills theory*, *Phys. Rev. D* **50** (1994) 266 [[hep-ph/9307356](#)].
  - [29] A. Ringwald, *An Upper bound on the total cross-section for electroweak baryon number violation*, *JHEP* **0310** (2003) 008 [[hep-ph/0307034](#)].
  - [30] L. A. Anchordoqui, H. Goldberg, D. Gora, T. Paul, M. Roth, S. Sarkar and L. L. Winders, *Using cosmic neutrinos to search for non-perturbative physics at the Pierre Auger Observatory*, *Phys. Rev. D* **82** (2010) 043001 [[1004.3190](#)].
  - [31] L. A. Anchordoqui, *Ultrahigh Energy Cosmic Rays: Facts, Myths, and Legends*, CERN Yellow Report CERN-2013-003, 303 [[1104.0509](#)].
  - [32] B. Acharya *et al.* [MoEDAL Collaboration], *The Physics Programme Of The MoEDAL Experiment At The LHC*, *Int. J. Mod. Phys. A* **29** (2014) 1430050 [[1405.7662](#)].
  - [33] F. L. Bezrukov, D. Levkov, C. Rebbi, V. A. Rubakov and P. Tinyakov, *Semiclassical study of baryon and lepton number violation in high-energy electroweak collisions*, *Phys. Rev. D* **68** (2003) 036005 [[hep-ph/0304180](#)].
  - [34] F. L. Bezrukov, D. Levkov, C. Rebbi, V. A. Rubakov and P. Tinyakov, *Suppression of baryon number violation in electroweak collisions: Numerical results*, *Phys. Lett. B* **574** (2003) 75 [[hep-ph/0305300](#)].
  - [35] S. Dutta, D. A. Steer and T. Vachaspati, *Creating Kinks from Particles*, *Phys. Rev. Lett.* **101** (2008) 121601 [[0803.0670](#)].
  - [36] T. Romanczukiewicz and Y. Shnir, *Oscillon resonances and creation of kinks in particle collisions*, *Phys. Rev. Lett.* **105** (2010) 081601 [[1002.4484](#)].
  - [37] H. Lamm and T. Vachaspati, *Numerical Exploration of Soliton Creation*, *Phys. Rev. D* **87** (2013) 065018 [[1301.4980](#)].
  - [38] C. Papageorgakis and A. B. Royston, *Revisiting Soliton Contributions to Perturbative Amplitudes*, *JHEP* **1409** (2014) 128 [[1404.0016](#)].
  - [39] D. E. Morrissey, T. M. P. Tait and C. E. M. Wagner, *Proton lifetime and baryon number violating signatures at the CERN LHC in gauge extended models*, *Phys. Rev. D* **72** (2005) 095003 [[hep-ph/0508123](#)].

- [40] A. Brandenburg, A. Ringwald and A. Utermann, *Instantons in Lepton Pair Production*, Nucl. Phys. B **754** (2006) 107 [[hep-ph/0605234](#)].
- [41] G. Dvali, G. F. Giudice, C. Gomez and A. Kehagias, *UV-Completion by Classicalization*, JHEP **1108** (2011) 108 [[1010.1415](#)].
- [42] S. V. Demidov and D. G. Levkov, *Soliton-antisoliton pair production in particle collisions*, Phys. Rev. Lett. **107** (2011) 071601 [[1103.0013](#)].
- [43] V. G. Kiselev, *The False vacuum decay induced by a two particle collision in two-dimensions*, Phys. Rev. D **45** (1992) 2929.
- [44] V. A. Rubakov, D. T. Son and P. G. Tinyakov, *Initial state independence of nonperturbative scattering through thin wall bubbles in (1+1)-dimensions*, Phys. Lett. B **278** (1992) 279.
- [45] M. B. Voloshin, *Decay Of False Vacuum In (1+1)-dimensions*, Yad. Fiz. **42** (1985) 1017 [Sov. J. Nucl. Phys. **42** (1985) 644].
- [46] K. B. Selivanov and M. B. Voloshin, *Destruction Of False Vacuum By Massive Particles*, JETP Lett. **42** (1985) 422.
- [47] M. B. Voloshin and K. G. Selivanov, *On Particle Induced Decay of Metastable Vacuum*. (In Russian) Yad. Fiz. **44** (1986) 1336.
- [48] P. B. Arnold and M. P. Mattis, *Baryon Violation at the SSC? Recent Claims Reexamined*, Phys. Rev. D **42** (1990) 1738.
- [49] S. Y. Khlebnikov, V. A. Rubakov and P. G. Tinyakov, *Instanton induced cross-sections below the sphaleron*, Nucl. Phys. B **350** (1991) 441.
- [50] V. A. Rubakov, D. T. Son and P. G. Tinyakov, *Classical boundary value problem for instanton transitions at high-energies*, Phys. Lett. B **287** (1992) 342.
- [51] P. G. Tinyakov, *Multiparticle instanton induced processes and B violation in high-energy collisions*, Phys. Lett. B **284** (1992) 410.
- [52] A. H. Mueller, *Comparing two particle and multiparticle initiated processes in the one instanton sector*, Nucl. Phys. B **401** (1993) 93.
- [53] G. F. Bonini, A. G. Cohen, C. Rebbi and V. A. Rubakov, *The Semiclassical description of tunneling in scattering with multiple degrees of freedom*, Phys. Rev. D **60** (1999) 076004 [[hep-ph/9901226](#)].
- [54] D. G. Levkov, A. G. Panin, and S. M. Sibiryakov, *Signatures of unstable semiclassical trajectories in tunneling*, J. Phys. A: Math. Theor. **42** (2009) 205102 [[0811.3391](#)].
- [55] W. H. Press, S. A. Teukolski, W. T. Vetterling and B. P. Flannery, *Numerical Recipes in C: The Art of Scientific Computing*, Cambridge Univ. Press (1988).
- [56] S. V. Demidov and D. G. Levkov, to be published.
- [57] A. N. Kuznetsov and P. G. Tinyakov, *False vacuum decay induced by particle collisions*, Phys. Rev. D **56** (1997) 1156 [[hep-ph/9703256](#)].
- [58] W. H. Miller, *Semiclassical Treatment of Multiple Turning-Point Problems — Phase Shifts and Eigenvalues*, J. Chem. Phys. **48** (1968) 1651.

- [59] M. J. Davis and E. J. Heller, *Quantum dynamical tunneling in bound states*, *J. Chem. Phys.* **75** (1981) 246.
- [60] S. V. Demidov and D. G. Levkov, *Soliton pair creation in classical wave scattering*, *JHEP* **1106** (2011) 016 [[1103.2133](#)].
- [61] S. Y. Khlebnikov, V. A. Rubakov and P. G. Tinyakov, *Periodic instantons and scattering amplitudes*, *Nucl. Phys. B* **367** (1991) 334.
- [62] D. S. Gorbunov et al, *Valerii Anatol'evich Rubakov (on his 60th birthday)* *Phys. Usp.* **58** (2) (2015).